Multiyear measurements of the oceanic and atmospheric boundary layers at the Brazil-Malvinas confluence region

Luciano Ponzi Pezzi,[1] Ronald Buss de Souza,[2] Otávio Acevedo,[3] Ilana Wainer,[4] Mauricio M. Mata,[5] Carlos A. E. Garcia,[5] and Ricardo de Camargo[6]

[1] This study analyzes and discusses data taken from oceanic and atmospheric measurements performed simultaneously at the Brazil-Malvinas Confluence (BMC) region in the southwestern Atlantic Ocean. This area is one of the most dynamical frontal regions of the world ocean. Data were collected during four research cruises in the region once a year in consecutive years between 2004 and 2007. Very few studies have addressed the importance of studying the air-sea coupling at the BMC region. Lateral temperature gradients at the study region were as high as $0.3°C\ km^{-1}$ at the surface and subsurface. In the oceanic boundary layer, the vertical temperature gradient reached $0.08°C\ m^{-1}$ at 500 m depth. Our results show that the marine atmospheric boundary layer (MABL) at the BMC region is modulated by the strong sea surface temperature (SST) gradients present at the sea surface. The mean MABL structure is thicker over the warmside of the BMC where Brazil Current (BC) waters predominate. The opposite occurs over the coldside of the confluence where waters from the Malvinas (Falkland) Current (MC) are found. The warmside of the confluence presented systematically higher MABL top height compared to the coldside. This type of modulation at the synoptic scale is consistent to what happens in other frontal regions of the world ocean, where the MABL adjusts itself to modifications along the SST gradients. Over warm waters at the BMC region, the MABL static instability and turbulence were increased while winds at the lower portion of the MABL were strong. Over the coldside of the BC/MC front an opposite behavior is found: the MABL is thinner and more stable. Our results suggest that the sea-level pressure (SLP) was also modulated locally, together with static stability vertical mixing mechanism, by the surface condition during all cruises. SST gradients at the BMC region modulate the synoptic atmospheric pressure gradient. Postfrontal and prefrontal conditions produce opposite thermal advections in the MABL that lead to different pressure intensification patterns across the confluence.

Citation: Pezzi, L. P., R. B. de Souza, O. Acevedo, I. Wainer, M. M. Mata, C. A. E. Garcia, and R. de Camargo (2009), Multiyear measurements of the oceanic and atmospheric boundary layers at the Brazil-Malvinas confluence region, *J. Geophys. Res.*, *114*, D19103, doi:10.1029/2008JD011379.

1. Introduction

[2] The western region of the South Atlantic Ocean is highly complex in terms of ocean circulation, water masses formation, and mixing both at the open ocean and at the coast. The open ocean is modulated by strong mesoscale variability, mainly dominated by the Brazil Current (BC) and the Malvinas/Falkland Current (MC) at their meeting region known as the Brazil-Malvinas Confluence (BMC). These currents are characterized by high temporal and spatial variability of the transport, sea surface temperature (SST), chlorophyll concentration, and sea surface height. The BMC region is known as one of the most dynamically active regions of the world ocean [*Chelton et al.*, 1990; *Piola and Matano*, 2001]. When reaching the BMC region, the tropical/subtropical (warm) waters transported southward by the BC interact with the subantarctic (cold) waters transported by the MC in opposite direction. The mixing of these distinct water masses define the western end of the subtropical convergence in the South Atlantic, a region known for the formation and subduction of the South Atlantic Central Water (SACW). The last spreads itself all over the South Atlantic Ocean in subsurface layers. In

---

[1]Earth Observation General Coordination, National Institute for Space Research, São José dos Campos, Brazil.

[2]Southern Regional Center for Space Research, National Institute for Space Research, Santa Maria, Brazil.

[3]Department of Physics, Federal University of Santa Maria, Santa Maria, Brazil.

[4]Department of Physical Oceanography, University of São Paulo, São Paulo, Brazil.

[5]Ocean and Climate Studies Laboratory, Institute of Oceanography, Federal University of Rio Grande, Rio Grande, Brazil.

[6]Institute of Astronomy, Geophysics and Atmospheric Sciences, University of São Paulo, São Paulo, Brazil.

particular locations at tropical regions of the Brazilian coast, depending on the intensity and persistency of the prevailing northeastern winds, the SACW is upwelled bringing nutrient-rich waters to the continental shelf and promoting the establishment of well-known phytoplankton blooms [e.g., *Castro et al.*, 2006].

[3] The surface thermal contrasts between distinct water masses in the ocean are known to contribute toward the generation of intense momentum gradients and energy vertical fluxes between the ocean and the atmosphere. These fluxes affect the dynamical and thermodynamical structure of both ocean and atmosphere [*Chelton et al.*, 2001; *Hashizume et al.*, 2002; *Pezzi et al.*, 2004, 2005; *Tokinaga et al.*, 2005; *Spall*, 2007, *Small et al.*, 2008]. In addition to that, the turbulent processes occurring at small spatial and temporal scales (order of kilometers and hours) may induce variations on the evolution of large-scale processes [*Pezzi and Richards*, 2003], at the order of thousands of kilometers and several days. The large-scale processes have direct influence on the meteorological and oceanographic processes affecting the South American coastal region [*Gan and Rao*, 1991; *Hoskins and Hodges*, 2005].

[4] Not long ago, *Xie* [2004], and recently, *Small et al.* [2008], have made comprehensive reviews of previous studies concerning the ocean-atmosphere (OA) interactions. The authors focused especially on areas of strong oceanic fronts such as the equatorial Pacific cold tongue [*Chelton et al.*, 2000; *Liu et al.*, 2000; *Polito et al.*, 2001; *Pezzi et al.*, 2004], the equatorial Atlantic [*Hashizume et al.*, 2001; *Caltabiano et al.*, 2005], and the Southern Ocean [*O'Neill et al.*, 2003]. Those reviews emphasized the necessity to study the coupling mechanisms between ocean and atmosphere at oceanic frontal regions. The authors pointed out the fact that over cold waters (where deep atmospheric convection does not occur), the OA interactions differ markedly from those occurring over warm waters. In this last case, many examples taken from *Xie* [2004] and *Small et al.* [2008] describe that the marine atmospheric boundary layer (MABL) becomes unstable and is deepened over warm surface waters. The turbulence and the vertical mixing within the vertical atmospheric column increases. As a consequence, the vertical shear decreases, and the surface winds become stronger over warm waters. Over colder waters an opposite situation is observed: the MABL is often more stratified and the surface winds are weaker.

[5] In a recent study, *Tokinaga et al.* [2005] provided a detailed analysis of the climatological characteristics of the surface atmospheric stability at the BMC region. The authors showed that there is a positive correlation between SST and surface wind speed at this region. Their findings were corroborated by *Pezzi et al.* [2005], and both are consistent with the mechanism proposed by *Wallace et al.* [1989], suggesting that the strong meridional SST gradient between BC and MC waters affects the vertical atmospheric mixing. This in turn will affect the MABL stability and will modulate the winds at lower atmospheric levels.

[6] Although the ocean-atmosphere coupling mechanisms, such as the vertical mixing, in the BMC region can be expected to mirror the behavior of other oceanic regions such as the equatorial Pacific and others, no observational data of the atmospheric and oceanic mixed layers structure (as well as of air-sea coupling parameters) are currently available for the BMC region to our knowledge. An exception to this is the pioneering work of *Pezzi et al.* [2005]. These last authors presented a description of both oceanic and atmospheric boundary layers from observations made during a single research cruise at the BMC region in November 2004. Nevertheless, simultaneous descriptions of the synoptic conditions of the MABL and of the oceanic boundary layer (OBL) are still very rare for the BMC region as well as for the whole of the South Atlantic Ocean.

[7] This paper extends the previous work made by *Pezzi et al.* [2005] and presents a synoptic description of the MABL and OBL structure as well as the air-sea coupling at the BMC region. The work is based on in situ data collected during four research cruises performed during specific dates in the austral spring from 2004 to 2007. The paper is outlined as follows: section 2 presents the sampling design, the in situ data, and the applied methodology. A synoptic analysis of the atmosphere and the ocean at the experimental period is made in section 3. The OBL and MABL structure and the atmospheric adjustment to the oceanic front are discussed in section 4. The paper finishes with a section presenting our concluding remarks and suggestions for future studies.

2. Data and Methods
2.1. In Situ Data Collection

[8] In order to better understand the temporal and spatial variability of the oceanographic processes and properties occurring in the southwestern Atlantic and their relationship to the Southern Ocean variability, a research program was established in Brazil in 2002 under the umbrella of the Brazilian Antarctic Program (PROANTAR). Most of the projects in the field of oceanography were headed by a research group called the High Latitudes Oceanography Group (GOAL). The research group has, among others, the objective of investigating the kinematics and dynamics of the BMC region and their relation to the Antarctic and Subantarctic environments. The program for measuring and analyzing the air-sea interactions under the GOAL program is specifically named Air-Sea Interaction at Brazil-Malvinas Confluence (INTERCONF). One of its objectives is the investigation of the air-sea coupling in the BMC region and its impact on the weather and climate of the adjacent South America coastal regions.

[9] During a sequence of INTERCONF cruises during austral spring, simultaneous oceanic and atmospheric observations were made onboard the Brazilian Navy Oceanographic Support Ship (OSS) *Ary Rongel* while crossing the BMC region. In this study we present an interannual analysis of the MABL thermal structure mostly based on vertical profiles collected during four cruises between the years of 2004 to 2007. During the cruises, data for both MABL and oceanic boundary layer (OBL) were obtained in the BMC region. The in situ experiments were inspired by previous works where the air-sea coupling was investigated at oceanic frontal regions in the equatorial Pacific [*Hashizume et al.*, 2002], in Agulhas Current return flow [*Rouault et al.*, 2000], and in the BMC region itself [*Pezzi et al.*, 2005; *Tokinaga et al.*, 2005].

[10] The OSS *Ary Rongel* departs from Brazil toward Antarctica every year during the austral spring. Prior to the

ship's departure from the port of the Rio Grande city in southern Brazil, the position of the BC return flow at the BMC region is mapped. The strong surface thermal gradients between BC and MC in the region are determined by satellite imagery and guide the ship toward the region of maximum thermal gradients between BC and MC (BC/MC front).

[11] The study area of the experiments described here is located between 30° to 50°S and 50° to 60°W (Figure 1). This area was covered during specific dates from 2004 to 2007 as indicated in Table 1. While crossing the BC/MC front, Expendable Bathy-Thermographs (XBTs) were launched from the ship in order to measure the water temperature as a function of depth along the ship's route. When at the close vicinity of the front (Figure 1 and Table 3), a sequence of Vaisala (RS80 and RS90) radiosondes were also launched from the rear deck of the ship. The radiosondes measured pressure, temperature, and relative humidity (RH) in the atmosphere. Wind speed and direction were also estimated from the relative movement of the radiosonde balloon in the atmosphere. The measurements were made at regular intervals of 2 s, which guaranteed a fair number of observations within the MABL, with vertical resolution varying from 7 to 10 m in the first kilometer of the MABL height. The position of the radiosonde balloons was traced with the help of a Global Position System (GPS) device onboard of the ship. Other atmospheric variables were automatically derived by the radiosonde receptor in real time: potential temperature (θ), dew point temperature (T_d), ascension rate, geopotential height, and mixing ratio or specific humidity (q).

[12] Before each radiosonde ascent, a ground (onboard) check was made in order to obtain correction values for the primary measurements of each radiosonde. During that check, the humidity sensor was placed in a tight sealed dry chamber, and the sensor humidity was adjusted to zero percent. The temperature was measured by an independent thermometer and checked against the radiosonde measurement. In situ independent measurements made by the ship's meteorological station were used to correct for ground check differences. After this procedure, the onboard receptor was synchronized with the radiosonde, which was attached to a balloon for release. The radiosondes were launched when the ship was crossing over from the BC (warm waters) to the BC/MC front and then to the MC (cold waters), respectively launching as many radiosondes as possible in a period of up to a day. The XBTs were launched simultaneously with the radiosondes in distances close to a quarter degree latitude.

2.2. Satellite and Atmospheric Data

[13] A number of different data sources were employed over the course of this investigation. As the atmospheric conditions during the experiments were mostly cloudy, the synoptic thermal surface structure of the BMC region could not be observed by infrared imagery. However, satellite microwave data from the Advanced Microwave Scanning Radiometer onboard the EOS-Aqua satellite (AMSR-E) was fully available for the date of the experiments with no cloud contamination. The Aqua satellite is polar orbiting, offering a global coverage of the planet.

[14] AMSR-E is a 12-channel passive microwave radiometer (6.9, 10.7, 18.7, 23.8, 36.5, and 89.0; vertical and horizontal polarizations). Raw data is processed into SST at Remote Sensing Systems (RSS) that is a NASA partner for data processing and distribution. Global AMSR-E SST data are available on a daily basis at the RSS Web site (http://www.rems.com) as well as wind vectors from the QuikScat scatterometer. *Wentz et al.* [2003] performed a preliminary validation of the AMSR-E SST against Reynolds Optimum Interpolation (OI) weekly SST. The root mean square error (RMS) differences between AMSR-E and OI SST were 0.76°C over a 3-month period spanning from June to August 2002. The nominal spatial resolution of the RSS AMSR-E global product is 25 km. A more recent evaluation of the AMSR-E accuracy is presented by *Chelton and Wentz* [2005].

[15] Gridded analysis data from the National Centers for Environmental Prediction (NCEP) Global Forecast System (GFS) at 1° grid spacing were used for all diagnostics of the atmospheric synoptic conditions occurring during the experiments (e.g., Figure 2). Also, GOES Imager infrared images for the period of all the experiments (several images per day in the period of the study) were obtained from the Brazilian Center for Weather Forecast and Climate Studies (CPTEC, http://www.cptec.inpe.br) and used in order to complement the synoptic analysis (not shown here).

2.3. Surface Bulk Flux Calculation and Stability Parameters

[16] From the raw radiosonde data, the turbulent fluxes of latent heat (Q_L) and sensible heat (Q_S) were calculated following the scheme proposed by *Fairall et al.* [1996]. A comprehensive description of the method is offered by those authors. The method was developed specifically with the Tropical Ocean Global Atmosphere–Coupled Ocean-Atmosphere Response Experiment (TOGA-COARE) data. The basic structure of the *Fairall et al.* [1996] algorithm follows the well-known Liu-Katsaros-Businger scheme and includes a different specification to the stress/roughness relationship. This approach considers the roughness due to the gravity waves and molecular viscosity [*Smith et al.*, 1996]. The humidity, temperature, and momentum profiles as a function of the stability under very unstable conditions are modified to adjust to the *Panofsky and Dutton* [1984] free convection scheme. The bulk formulas allow that sensible, latent heat and momentum fluxes can be estimated from the observed variables at 2 or 10 m (reference-level z_r). The basics of this scheme are presented below [*Fairall et al.*, 1996]:

$$Q_S = \rho c_p C_h U(\theta_{air} - SST) \qquad (1)$$

$$Q_L = \rho L_e C_e U(q_s - q_{air}) \qquad (2)$$

where C_h and C_e are the heat and humidity transfer coefficients, which depend on atmospheric stability and are given by similarity relationships. θ_{air} is the potential temperature, q_s is the specific humidity at sea level, and q_{air} is the specific humidity at z_r. U is the mean speed of surface winds relative to the sea surface. All these variables
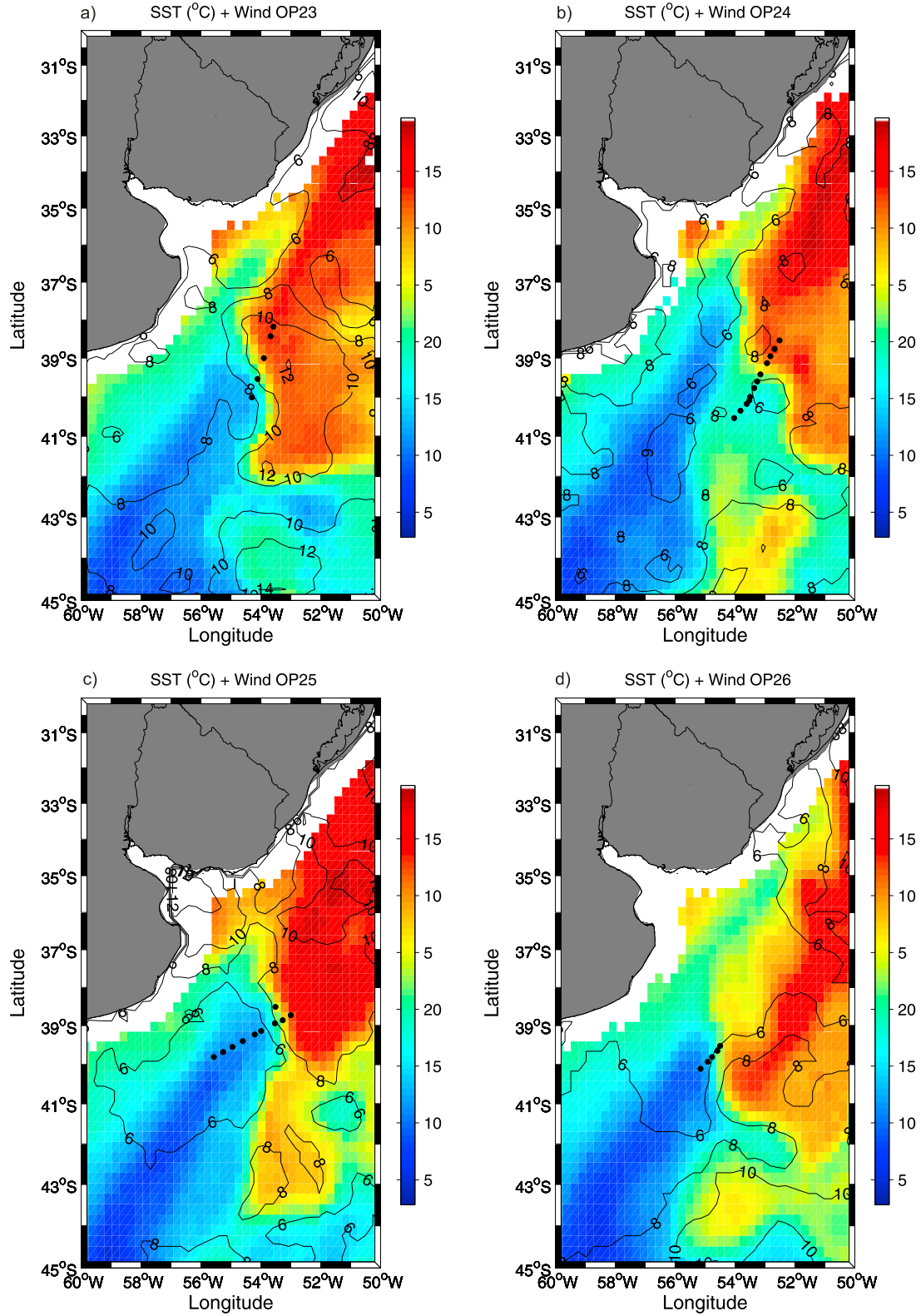
Figure 1. Brazil-Malvinas Confluence (BMC) study area with cruise routes, radiosonde ascent positions (black circles), and thermal front positions. QuikScat wind speeds (m s^{-1}) are the lines superimposed onto AMSR-E sea surface temperature (SST) images. All data are coincident in time with the experiments. The color bar denotes SST in °C. Experiments are from (a) OP23, (b) OP24, (c) OP25, and (d) OP26 routes.

Table 1. Experiment Names and Dates

Experiment Name	Date
OP23	2 to 3 November 2004
OP24	28 to 29 October 2005
OP25	27 to 28 October 2006
OP26	16 to 17 October 2007

are measured at z_r. In this study we also evaluate the total heat flux (Q_T) as given as

$$Q_T = Q_L + Q_S \qquad (3)$$

The induced additional flux due to the scale variability of the boundary layer and considering the gustiness effect is

also taken into account. The scaling parameter L defined as the Obukhov length is also calculated by the *Fairall et al.* [1996] algorithm. According to *Stull* [1988], the physical meaning of this parameter is that L represents the height in the boundary layer at which buoyant factors first dominate turbulence produced by mechanical factors, e.g., shear. An atmospheric boundary layer stability parameter at 10-m height (ζ) is derived using L:

$$\zeta = 10/L \qquad (4)$$

where $\zeta < 0$ means statically unstable (negative) and $\zeta > 0$ means statically stable (positive) conditions.
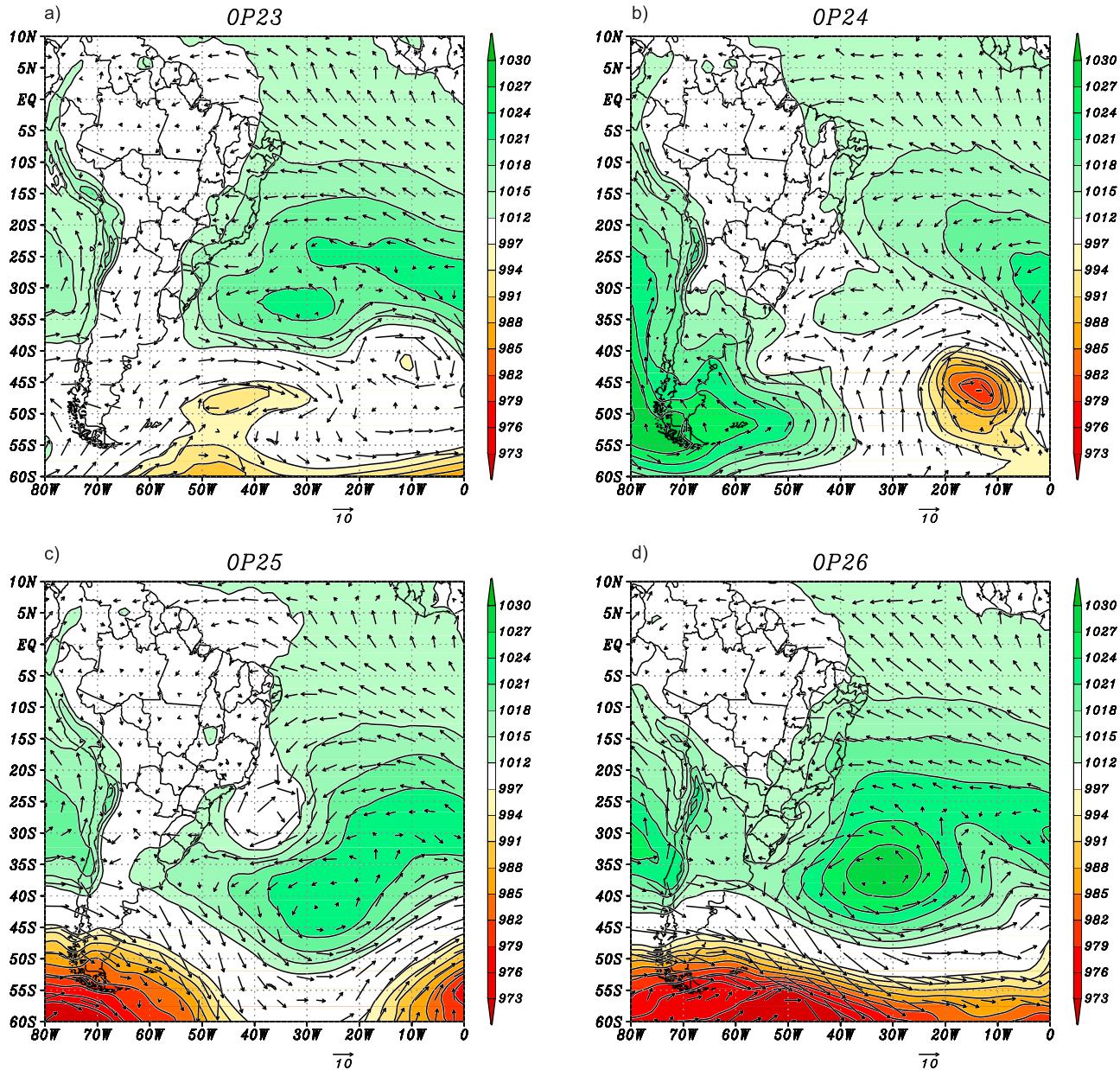

Figure 2. Surface synoptic weather analysis, averaged over 0000 and 1200 GMT. Sea-level pressure (hPa) with surface wind (m s^{-1}) vectors superimposed for (a) OP23, 3 November 2004; (b) OP24, 28 October 2005; (c) OP25, 16 October 2006; and (d) OP23, 27 October 2007.

Table 2. Description of Quantities Used in the Radiosonde Profiles Normalization on θ, q, and *RH* Composites Calculation and Horizontal and Vertical Temperature Gradients[a]

OP	$h_{0\mathrm{warm}}$	$h_{0\mathrm{cold}}$	θ_{warm}	θ_{cold}	q_{warm}	q_{cold}	ΔT_{hor}	ΔT_{ver}
OP23	280	235	17.2	13.0	8.9	6.7	0.03 (39.0°S)	0.08 (39.0°S-400 m)
OP24	700	500	10.1	8.6	3.9	3.9	0.03 (39.2°S)	0.09 (39.4°S-400 m)
OP25	800	250	14.7	12.6	6.9	6.5	0.05 (38.8°S)	0.07 (39.4°S-400 m)
OP26	1060	250	15.2	11.3	7.8	7.6	0.01 (39.8°S)	0.09 (39.6°S-200 m)

[a]OP is the experiment name. Included are the top marine atmospheric boundary layer (MABL) height for the warm ($h_{0\mathrm{warm}}$) and cold ($h_{0\mathrm{cold}}$) composites; mean MABL potential temperature for the warm (θ_{warm}) and cold (θ_{cold}) composites; mean MABL specific humidity for the warm (q_{warm}) and cold (q_{cold}) composites (units are meters for h, °C for θ, and g/kg for q); the horizontal temperature gradient (ΔT_{hor}) at sea surface with the latitude indicated in the parentheses, and the vertical temperature gradient (ΔT_{ver}) with the latitude and depth indicated in parentheses (both gradients are in °C m^{-1}).

[17] It is important to remark that the *Fairall et al.* [1996] scheme was originally developed to be used on turbulent fluxes over the warm pool in the western Pacific Ocean at the COARE study region. However, *Fairall et al.* [1996] argues that this scheme has also included extra-tropical data from other research programs. An update version of the original algorithm was proposed by *Fairall et al.* [2003] where the authors present the COARE algorithm version 3.0. Therefore, this model is considered to be suitable for extratropical studies as in our case, being even used in the past for polar regions [*Fairall et al.*, 1996]. The method is largely used by others authors at oceanic frontal regions, e.g., *Rouault et al.* [2000] at the Agulhas Current.

[18] Another parameter widely used for estimating the near-surface stability is obtained by computing the difference between the SST and the near-surface air temperature [*Pezzi et al.*, 2005; *Tokinaga et al.*, 2005]. Both variables were routinely recorded in shipboard observations. In this work, the stability parameter is defined as $\mathrm{SST}_{\mathrm{bulk}} - T_{\mathrm{ship}}$, where $\mathrm{SST}_{\mathrm{bulk}}$ is the bulk-based, in situ manually collected SST by the OSS *Ary Rongel* crew along the ship route, and T_{ship} is the air temperature. These observations were collected at enough spatial and temporal resolutions to allow us the construction of high-resolution data sets. These data sets were used to investigate the MABL stability adjustment to the strong BC/MC front thermal gradients and test the vertical-mixing mechanism. T_{ship}, sea-level pressure (SLP), and RH were measured by the meteorological weather station located at the upper level of the ship, at 11 m above the sea surface. Wind speed measurements ($\mathrm{Wind}_{\mathrm{ship}}$) were made at 22 m. All calculations using the meteorological weather station data are hourly averages.

2.4. MABL Composites

[19] The mean MABL structure is described with vertical structure composites (averages) of the radiosondes profiles calculated using a similar strategy of *Pyatt et al.* [2005]. The composite method was applied for each transect accomplished during the four experiments. The radiosonde data were grouped as a function of their location relative to the SST gradients at the BMC region. Because of the nature of the main currents in the area, the warm (cold) waters are always located northward (southward) of the BC/MC front. For example, during the first experiment (OP23) in the spring of 2004, five radiosondes were launched (Figure 1a). Three of them were released over the warmside of the front, being then used to calculate what we define here as the warm composite of the MABL vertical structure. The other two ascents over the coldside of the front were used to get

the cold composite of the OP23. Warm and cold composites were computed for all four experiments.

[20] In order to obtain an accurate description of the vertical structure for this composite analysis, the soundings made at the northern (warm) part of the front and at the southern (cold) part of the front were independently averaged, generating averaged profiles for the warm and cold regions. At each averaged profile, the MABL top height (h_0), was subjectively determined using both q and θ profiles. This is the region where the capping inversion layer or entrainment zone lies. The average h_0 values for all experiments are indicated in Table 2. According to *Stull* [1988], we can assume that the parameters q and θ are well mixed within the MABL and remain approximately constant (adiabatic) in the mixed layer. MABL height depends on the turbulent mixing. A strong gradient of q and θ is observed at higher levels of the atmospheric profile when the inversion layer is reached. After that level, the inversion layer and the h_0 are determined by the point when an abrupt change occurs on the profiles, with θ increasing and q decreasing [*Fisch et al.*, 2004]. When this criterion is not met, *Santos* [2005] suggests the use of the θ profiles to determine h_0 as errors or malfunctions are more common on humidity sensors than on the temperature ones. A similar approach is also used by *Albrecht et al.* [1995]. Over the coldside of the confluence, especially in cases with warm-air advection, a very stable layer is observed above the surface. Nevertheless, above this layer, it is possible to observe a less stable layer, capped by a stronger inversion. In such cases, this upper inversion was considered as the MABL height. The MABL top height determination using θ_v was investigated, and it did not show significant differences with respect to calculations using θ.

[21] The vertical composites were obtained using a non-dimensional height scale. According to *Albrecht et al.* [1995] and *Pyatt et al.* [2005], this procedure preserves the MABL structure and the inversion height (h_0) main characteristics even if there are no changes from one sounding to another. This is implemented by normalizing the radiosondes height (h) by the mean top MABL height of the warm and cold portions separately, $\overline{h_0}$,

$$h_* = h/\overline{h_0} \qquad (5)$$

[22] This procedure actually transforms h in a nondimensional vertical axis (h_*). After this step, we look at the average profile from the surface to $\overline{h_0}$ and computed perturbations, which are the differences of each variable to the mean profiles within the MABL. Those mean values

were calculated for the cold and warm cases, as seen in Table 2. After that, the composites were calculated as well as the averaged perturbations of each variable throughout the four experiments. The variables were finally restored by multiplying the vertical coordinate by the mean h_0 and then adding the mean values of each variable to the composited perturbations. The analysis of the MABL presented here is restricted to the first 1200 m from the sea surface.

3. Synoptic Analysis

3.1. Oceanic Synoptic Analysis

[23] In order to present a wider view of the oceanic characteristics of the study region, the synoptic conditions present on the four INTERCONF cruises are shown in Figure 1. Figure 1 shows AMSR-E derived SST fields with near-surface QuikScat wind vectors superimposed. The distribution of the warmer BC waters (in tones ranging from yellow to red) and of the colder MC waters (in blue to green) can be easily seen in the images. The meeting location of the opposite Brazil and Malvinas currents is noticed by strong SST gradient typical of the encounter between both currents in the area. The location of the front in the BMC region responds to the mesoscale variability of the confluence as well as the large-scale climatic (atmospheric and oceanic) regime which has strong seasonal behavior [Legeckis and Gordon, 1982].

[24] Figure 1 also indicates with black circles the radiosonde-launching positions during all cruises. From these positions the ship routes crossing the BC/MC front can be approximately inferred. The tracks representing the ship's routes indicate that the BC/MC front was consistently crossed at about 39°S to 40°S and 53°W to 54°W. Systematically, in all cruises the SST reached a maximum of approximately 20°C over the BC warm core. On the other hand, the SST values dropped down to values near 5°C over the cold core of the MC. This remarkable surface SST gradient is present during the four experiments and agrees with descriptions made for the BMC by many authors [e.g., Legeckis and Gordon, 1982; Garcia et al., 2004; Souza et al., 2006]. Another remarkable synoptic characteristic of the study area clearly seen in Figure 1 is that the wind speed tends to adjust to the SST field at BC/MC front. Wind speed minima are observed over the cool water at the MC core. In opposition to that, winds are quite strong away from the MC core in coastal regions and over the BC warm waters. This synoptic pattern of wind modulation agrees with the annual climatology presented by Tokinaga et al. [2005] for the BMC region.

[25] It is also worth remarking that several cyclonic (clockwise in the southern hemisphere) and anticyclonic (anticlockwise) eddies are continuously shed from the MC and from the BC, respectively. They are three-dimensional structures that can easily be identified in SST satellite images for their warm (cold) signatures on cold (warm) waters. Vertically, warm (cold) eddies act pushing (pulling) down (up) the thermocline. For instance, Souza et al. [2006] tracked a warm-core eddy shed by the BC in the BMC region assessing its lifespan and characteristics such as the heat and salt content, as well as the available potential energy. As the structures can persist for up to 3 months as they travel over the mean flow in the southwestern Atlantic,

they are considered an important player on the salt and heat balance of the region. During the analyzed period it was possible to identify some of those warm-core structures which can be associated to either shedding eddies or the meandering of the BC. It is out of the scope of this study to discuss the exact classification of those structures here; instead we want to remark that our data suggest that the wind speed over these oceanic features follows the same modulation pattern described before for the BC/MC front itself. Very discernable warm-core eddies are found in the study area during the OP24, OP25, and OP26 experiments, all centered around 39°S and 53°W. All of these eddies are associated to stronger winds (9 to 10 m s^{-1}) at the atmosphere over them. On the other hand, weaker winds are noticed over cold-core eddies. This is the case observed during OP25 where a 6 m s^{-1} wind speed is estimated over a cold eddy located at 42°S, 51°W.

3.2. Atmospheric Synoptic Analysis

[26] During the OP23 (2–3 November 2004) according to onboard observations, the sky was almost fully covered with clouds when the radiosondes were released. These observed clouds were mainly associated with instabilities produced by the subtropical jet stream and to a weak trough, both diagnosed by satellite images (not shown) and the surface synoptic charts seen in Figure 2a. A low-pressure system was located in the region between 45°S and 60°W, positioned to the east of the ship's route. This low pressure was associated with a weak frontal system that was crossing the region at the south. A satellite image animation (not shown) and a sea-level pressure chart of the period also showed that the large-scale northerly winds associated to the quasi-permanent Atlantic anticyclone were prevailing over most of the experiment area. This fact is reinforced by the in situ SLP observations made along the OSS Ary Rongel route and exhibited in Table 3. The data demonstrate that there was not any significant change on the measured SLP values compared to the ones measured by the radiosondes.

[27] The OP24 (28 October 2005) was performed under totally cloud covered conditions. This was mostly due to the presence of a low-pressure system located right over the route of the OSS Ary Rongel (Figure 2b). Although weak, this system was responsible for the observed cloudiness during OP24. Even in the presence of this system, the SST frontal gradient caused an impact on the SLP of the region. This is better discussed later in section 4.4 of this work (see Figure 7 and Table 3).

[28] During OP25 (27 October 2006), a low pressure with an associated frontal system was centered over the Malvinas (Falklands) Islands. The frontal system extended northward to the Malvinas Islands reaching the vicinity of the La Plata River. This frontal system was covering a large part of the sampling route of the ship during OP25 (Figure 2c). It is interesting to note that this experiment had a high-pressure system in the vicinity of the ship's route and a low-pressure system to the south of it. Besides the situation observed in the synoptic chart and satellite imagery of 27 October 2006, this fact is also corroborated by the SLP measurements taken onboard the ship. The measurements indicate higher SLP values over warmer waters while the opposite occurs over cold waters. A similar synoptic situation and SLP behavior were observed during OP26 (16 October 2007) as

Table 3. Experiments Name, Date, and Locations of the Radiosondes Ascent[a]

OP	Date	Time (LT)	Lat (S)	Lon (W)	SST_{Sat}	T_{air}	SLP_{Rad}	$Wind_{Rad}$	$Wind_{Sat}$
OP23	2 November 2004	1930	38.12	53.55	17.40	19.40	1010.0	10.00	8.80
	2 November 2004	2130	38.43	53.68	17.10	16.50	1007.0	10.00	9.00
	3 November 2004	0022	39.00	53.89	16.65	18.00	1006.0	7.00	9.20
	3 November 2004	0220	39.54	54.11	13.20	11.00	1007.0	5.00	8.80
	3 November 2004	0518	40.01	54.30	9.75	10.00	1008.0	7.00	5.80
OP24	28 October 2005	0232	38.63	52.58	16.65	15.00	1009.0	10.00	7.60
	28 October 2005	0329	38.76	52.68	16.95	14.00	1008.0	6.00	7.20
	28 October 2005	0451	38.95	52.82	17.25	14.00	1008.0	7.00	7.40
	28 October 2005	0714	39.27	53.02	16.65	12.00	1008.0	5.00	7.00
	28 October 2005	0811	39.42	53.15	14.70	12.00	1010.0	5.00	6.40
	28 October 2005	0916	39.60	53.26	12.60	10.00	1010.0	5.00	5.60
	28 October 2005	1024	39.77	53.36	11.40	14.50	1009.0	4.00	5.80
	28 October 2005	1201	40.00	53.50	10.95	15.00	1010.0	4.00	6.60
	28 October 2005	1322	40.04	53.52	10.95	15.00	1010.0	4.00	6.60
	28 October 2005	1421	40.18	53.61	10.95	15.00	1010.0	4.00	6.60
	28 October 2005	1619	40.35	53.82	11.10	14.00	1010.0	4.00	7.00
	28 October 2005	1746	40.54	54.03	11.25	11.50	1010.0	4.00	7.20
OP25	27 October 2006	1101	38.51	53.51	13.80	17.50	1014.2	13.00	8.20
	27 October 2006	1351	38.73	53.00	17.55	18.00	1016.0	5.00	9.40
	27 October 2006	1502	38.86	53.27	15.15	20.00	1015.0	6.00	8.80
	27 October 2006	1615	38.94	53.53	12.75	20.00	1015.0	6.00	7.60
	27 October 2006	1812	39.14	53.99	10.20	13.50	1013.0	3.60	5.60
	27 October 2006	1913	39.23	54.20	9.15	13.00	1013.0	4.10	5.40
	27 October 2006	2104	39.40	54.60	8.70	13.00	1012.0	5.10	4.60
	27 October 2006	2247	39.55	54.95	8.55	10.00	1012.0	5.10	4.40
	28 October 2006	0022	39.68	55.26	8.70	10.00	1012.0	8.20	4.20
	28 October 2006	0153	39.81	55.57	8.40	10.00	1011.0	8.20	4.00
OP26	16 October 2007	0512	39.52	54.50	13.05	11.00	1015.0	8.70	6.40
	16 October 2007	0706	39.68	54.62	13.05	14.00	1013.0	10.00	6.40
	16 October 2007	0806	39.81	54.77	10.65	14.00	1013.0	9.00	5.60
	16 October 2007	0852	39.93	54.91	8.85	12.00	1010.0	10.00	4.60

[a]The variables are air temperature (T_{air}) in °C, sea-level pressure (SLP_{Rad}) in hPa, and wind speed ($Wind_{Rad}$) in m s^{-1}. Data collected by the radiosondes on all experiments. AMSR-E sea surface temperature (SST_{Sat}) and QuikScat wind speed ($Wind_{Sat}$) are satellite data measurements approximately coincident with the radiosondes ascent time and positions. Note that T_{air} is the first-level radiosonde data.

shown in Figure 2d. In this last case, however, the high-pressure system was prevailing over the sampling region.

4. OBL and MABL Observations

4.1. OBL Mean Structure

[29] Figure 3 presents the simultaneous profiles of atmospheric potential temperature (θ) and ocean temperature taken along the route of the OSS *Ary Rongel* during the four INTERCONF cruises. Data were taken from the sequences of radiosonde and XBT measurements. Here we concentrate our analysis in the oceanic part of Figures 3a−3d where the temperature data collected with the XBTs are displayed as a function of depth. The OBL vertical structure shows that the sharp thermal gradients between BC and MC extend from the surface to about 500 m depth. These vertical and horizontal gradients characterize the very strong oceanic front of the BMC region. The estimated horizontal (ΔT_{hor}) and vertical (ΔT_{ver}) temperature gradients are shown in Table 2. ΔT_{hor} refers to the maximum horizontal gradient at the surface. ΔT_{ver} displayed in Table 2 refers to the maximum vertical gradient found in the BC/MC interface at depth. The latitude and depth where the maximum gradients were found are also indicated in Table 2. ΔT_{hor} was found to range from 0.01°C m^{-1} (OP26) to 0.05°C m^{-1} (OP25 at surface and at the vicinity of 39°S where the BC/MC front was located). The average gradient is 0.03°C m^{-1}. This value agrees with some early estimates

presented in the literature [e.g., *Garzoli and Garraffo*, 1989; *Saraceno et al.*, 2004; *Souza et al.*, 2006]. ΔT_{ver} ranged from 0.07°C m^{-1} to 0.09°C m^{-1} at 400 m depth, approximately, in most cases. At our study area, the surface subantarctic (MC) waters (colors ranging from blue to green in Figure 3) meet with the subtropical (BC) waters (colors ranging from yellow to red in Figure 3). At the confluence of those two water masses, mixing produces the South Atlantic Central Water which dives and spreads itself below the subtropical waters toward the north. The later water mass is associated to the thermal signature below 500 m in latitude lower than 39°S (Figure 3). *Bianchi et al.* [2002] reported the occurrence of a cross-frontal BC/MC interleaving, which produces the layering of relatively cold low-salinity waters over warm salty waters. This interleaving might be playing an important role on the BC/MC front, mixing physical properties by means of small-scale turbulent processes. Owing to their very high spatial resolution compared to previous hydrographical data presented in the BMC region, our temperature data (Figure 3a) were able to indicate the presence of mesoscale to small-scale structures at the subsurface in the ocean at the BC/MC front. These structures are particularly noticeable at approximately 39.5°S, confined to the first 400 m depth. In this case, some interleaving is clearly noticeable between the waters in the region. *Pezzi and Richards* [2003] demonstrated the strong influence of the lateral mixing enhancement at the vicinity of the equator in the Pacific Ocean. The physical
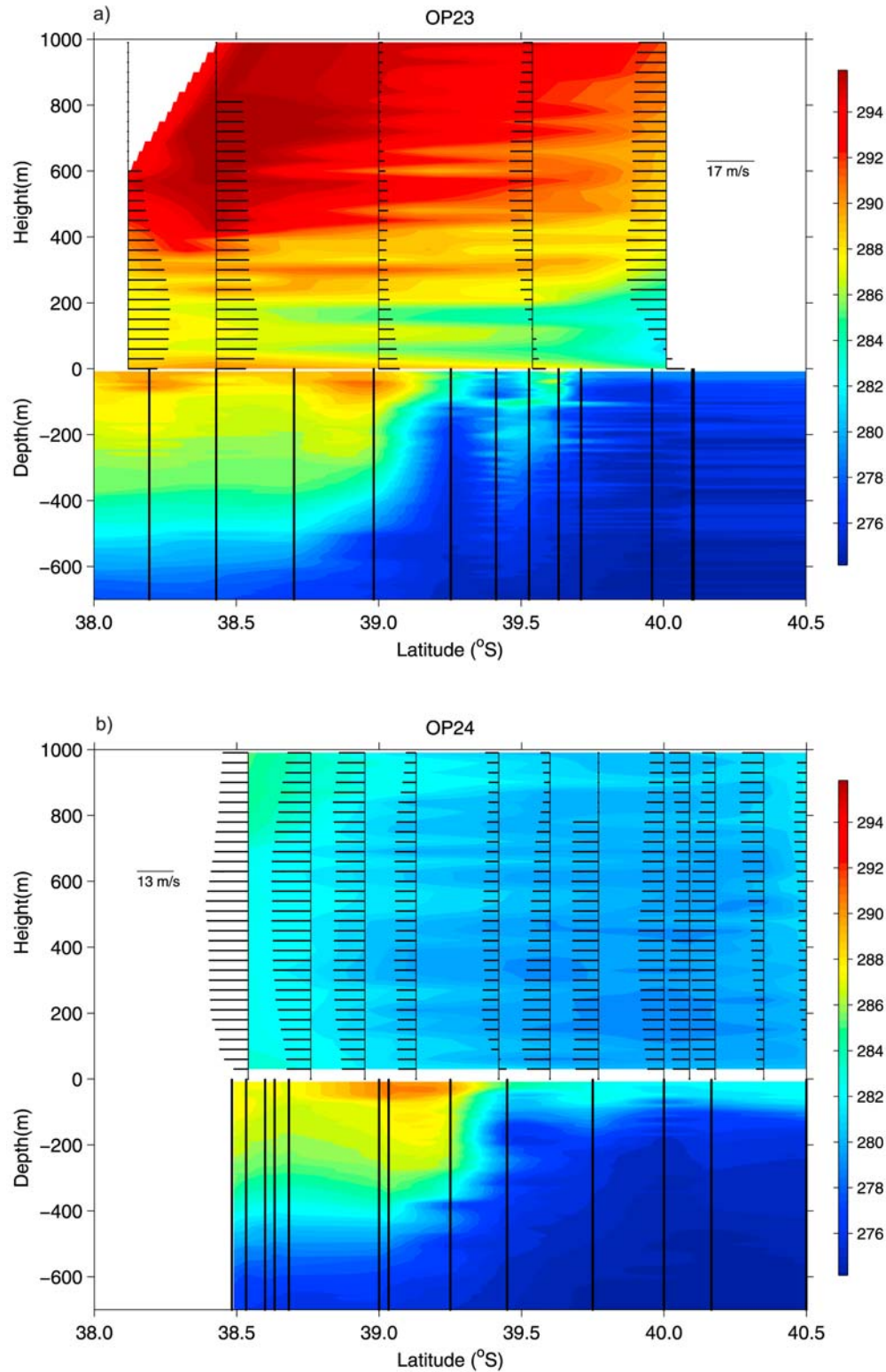
Figure 3. Temperature profiles (K) of the atmosphere and ocean taken simultaneously by radiosondes and XBTs along the OSS *Ary Rongel*'s routes during the four experiments OP23, OP24, OP25, and OP26. Meridional wind vectors (m s^{-1}) are also displayed. The profiles are for (a) 3 November 2004, (b) 28 October 2005, (c) 16 October 2006, and (d) 27 October 2007.

reasoning to which they have been based for explaining this enhanced mixing was the effect of the observed interleaving of water masses in producing a meridional flux of tracers and momentum at oceanic fronts [*Richards and Edwards*, 2003]. Although this process is likely to occur in the BMC as well, further study is necessary to better investigate the
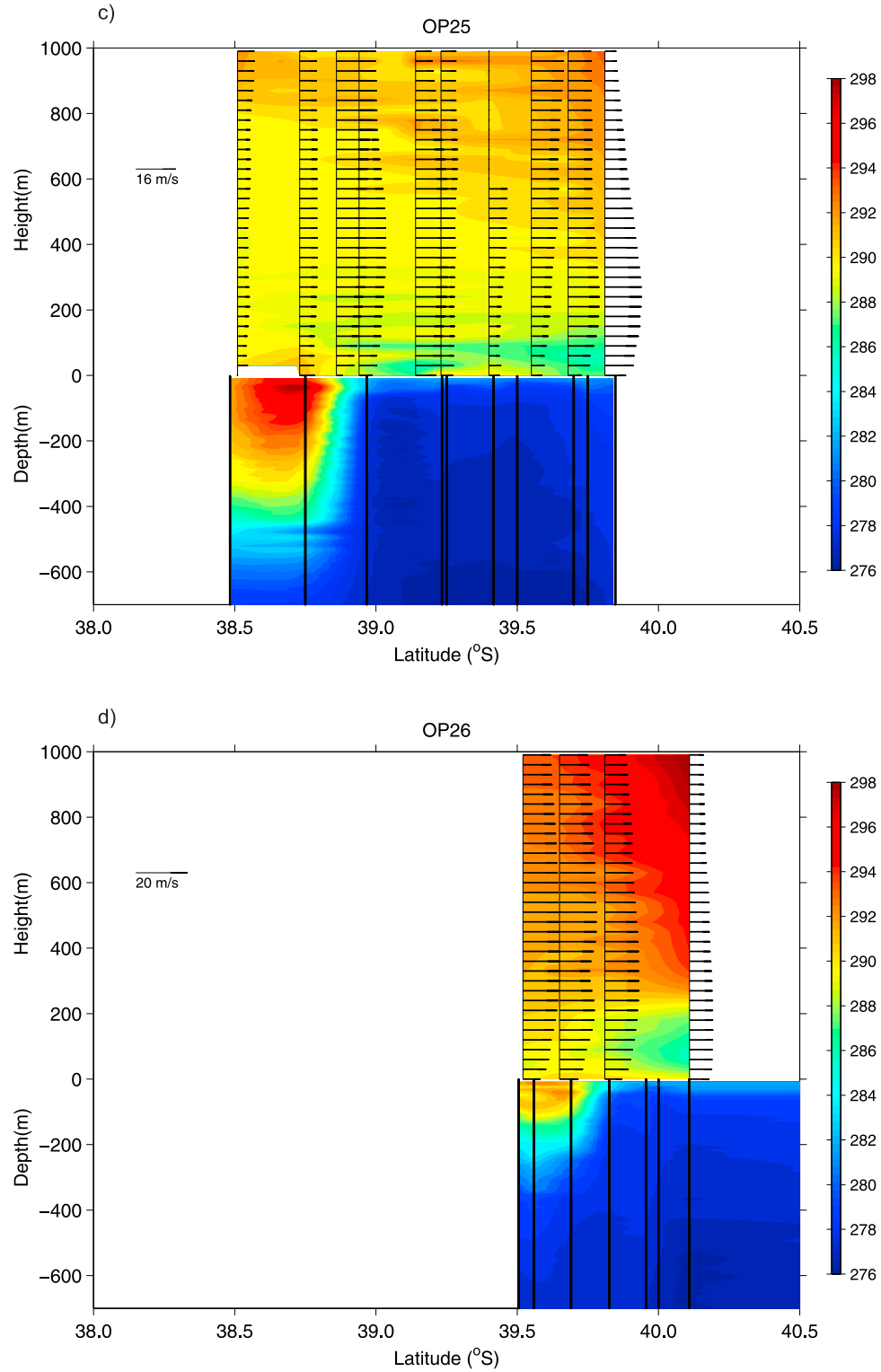
Figure 3. (continued)

characteristics and impacts of these small-scale features in the BMC zone.

4.2. MABL Mean Structure

[30] The thermal structure of the MABL, as measured by the radiosondes for each cruise, is displayed in the upper half of Figures 3a–3d. Figure 3 displays the atmospheric potential temperature (θ) together with the meridional wind also estimated from radiosonde data. Generally, at the south of the BC/MC front location, the air temperature is lower than at the north. Figure 3 clearly shows that MABL is being influenced by the OBL temperature distribution. Over the warm waters, we observe strong winds with an unstable mixed layer. On this side of the front, a reduction in the
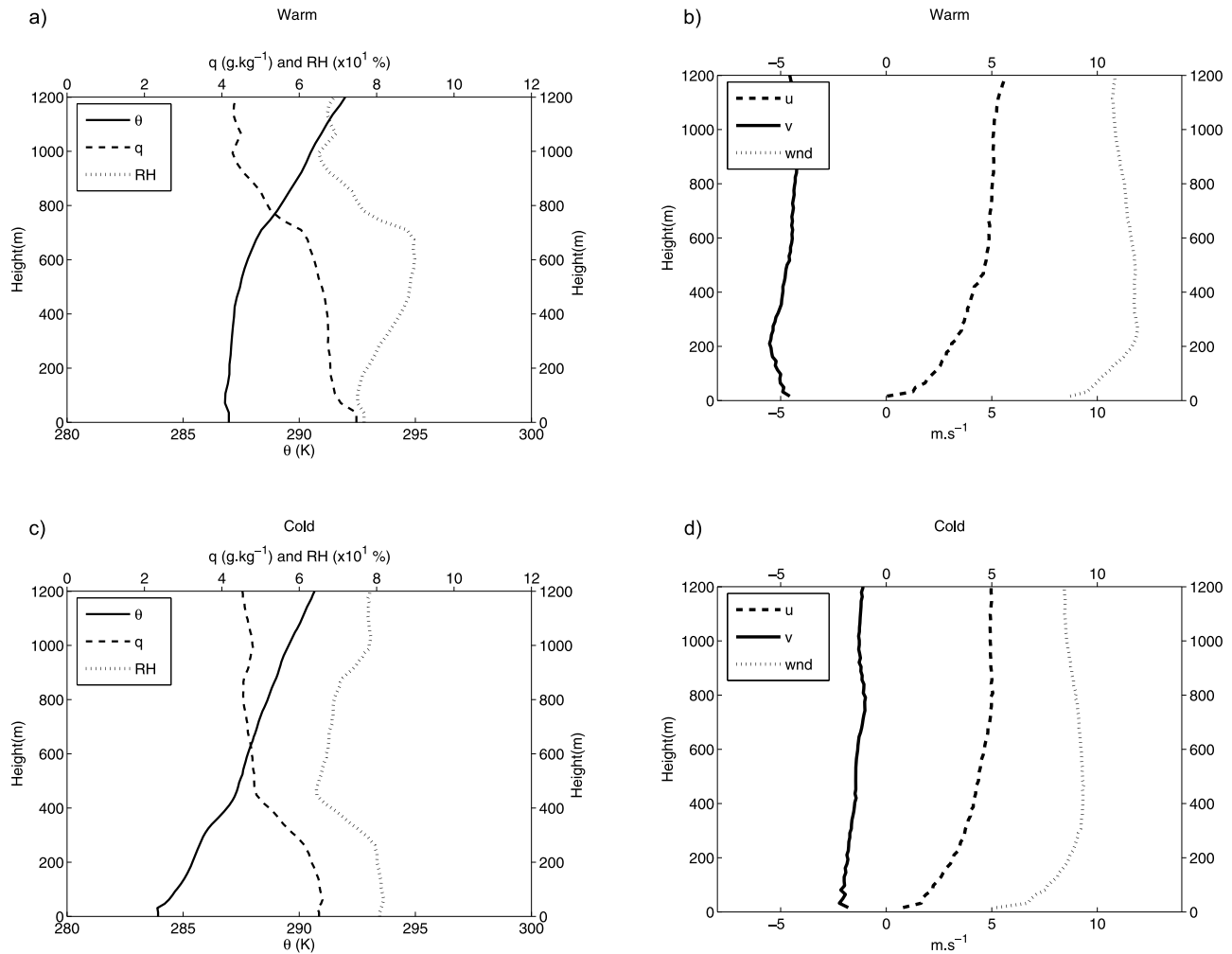
Figure 4. Vertical composite profiles of potential temperature (θ), specific humidity (q), and relative humidity (RH) for (a) warm and (b) cold cases. Vertical composite profiles of Wind speed (wnd) and zonal (u) and meridional (v) wind components for (c) warm and (d) cold cases.

wind shear and a decrease in the static stability of the near-surface atmosphere are also seen. Over the coldside of the front, on the other hand, the MABL is more stable, the wind shear is stronger, and the surface winds are weaker. Those signatures are consistent with the mechanism proposed by *Wallace et al.* [1989]. Still over cold waters, the atmosphere presents an increased vertical wind shear and a weakening of the surface winds. Our analysis shows that this vertical mixing mechanism occurring in the BMC region at synoptic time scale is in close agreement with the climatology described by *Tokinaga et al.* [2005]. Nearly all aspects of the ocean-atmosphere coupling observed in our results are also in agreement with previous studies made for other oceanic frontal regions, such as the eastern equatorial Pacific [*Wallace et al.*, 1989; *Hayes et al.*, 1989; *Chelton et al.*, 2001; *Hashizume et al.*, 2002; *Pezzi et al.*, 2004; *Small et al.*, 2005; *Spall*, 2007]. It is worth mentioning that the atmosphere at the BMC region responds to the strong SST gradients with a consequent strong horizontal thermal gradient (Figure 3). The radiosonde wind data is also in close agreement with the surface winds estimated from QuikScat measurements (Figure 2). The satellite-derived winds indicated that during three out of our four experi-

ments (OP24 is an exception), a predominant northerly meridional component was present along the ship's track where our in situ data were taken. Southern winds dominated the area during OP24. This information is crucial for understanding the mean characteristics of the MABL across the BC/MC front at BMC region. Distinct air temperature advection patterns take place depending whether the large-scale winds are blowing from the cold toward the warm region, or vice versa.

[31] Now we turn our attention to analyzing the vertical MABL structure as a function of the SST bottom boundary condition. Aiming for that objective, we use all radiosonde data collected in the four experiments. Figures 4a–4d display the composite calculations based on radiosonde vertical profiles of θ, q, RH, wind magnitude, and u and v wind components. The RH profiles were divided by 10^1 in order to plot q values in the same order of magnitude. The analyses presented here are restricted to the first 1200 m of height from the sea surface. These results are helpful to better understand the atmosphere characteristics as a function of the lower boundary surface. The composites of the atmosphere over warm waters (Figures 4a and 4b) show a well-defined convective MABL structure, including the top

height (h_0). The observed changes seen in the composites displayed in Figures 4a and 4c are consistent with the SST changes observed from the warmside to the coldside of the front. Figure 4a indicates that the MABL top was located at approximately 600 m. This feature is noticeable in both θ and q profiles. The humidity is well mixed at the warm region and does not present a strong vertical gradient. A strong thermal (θ) inversion occurs between 600 m and 800 m, after which a softer gradient is observed up to about 1600 m. At the lower levels inside the MABL, q remains almost constant with respect to height owing to the vertical turbulent mixing. In this case, a well-developed mixed layer takes place. The specific humidity decreases with height above h_0 (~600 m). This decrease is less intense than that of θ.

[32] Figures 4c and 4d show interesting features of the vertical composite profiles calculated over the coldside of the BMC region. These profiles display a lower MABL top with capping inversion at ~300 m height, where the atmosphere is becoming dryer (~60% of RH). At lower levels the RH is between 70% and 80%. Above the inversion level, q remains almost constant up to a secondary inversion level, which is detected at 700 m. The vertical structure of the inversions described here is observed in the RH and θ_e profiles. These profiles indicate a strong reduction of moisture, which originates at the sea surface and ascends toward the MABL. This fact suggests that the upper MABL is decoupled from the surface layer. *Hashizume et al.* [2002] observed a similar pattern over cold waters at the eastern equatorial Pacific. It should be noted that the θ profile cannot be used alone to clearly characterize the MABL top at our study region.

[33] Figures 4b and 4d show the composites of the vertical distribution of the zonal (u) and meridional (v) wind speed for the warmsides and coldsides of the BMC region. Figures 4b and 4d show that for both sides of the BC/MC front, the v component is negative indicating a wind flowing from the north along the whole of the MABL. The u component of the wind is positive at both sides of the front, indicating that westerly winds prevail. A minimum occurs at the surface. Near the surface, the northerly direction prevails on v. Above 400 m, the westerly direction dominates the u component of the wind. The larger magnitude of the northerly winds indicates that the large-scale synoptic circulation mostly prevailed during the period of our observations. For instance, Figure 2 shows that the surface northerly wind direction seen along the ship's route is associated to the high-pressure (anticyclonic) circulation present during OP23, OP25, and OP26. The meridional winds have larger magnitude compared to the zonal winds at BMC region. At the warm region of the oceanic front, the u component (and consequently the wind speed) is stronger at the surface when compared with the cold region (Figures 4b and 4d). Above 400 m, this situation is reversed: the u component (and wind speed) is weaker at the warm part of the front when compared to the cold part. This was not the case for v, which is strong throughout the whole of the MABL. The meridional component is high at both the warm and cold regions from the surface (−4.4 m s^{-1} and −4.2 m s^{-1}, respectively) up to 1200 m (−5.0 m s^{-1} and −1.6 m s^{-1}, respectively). A stronger vertical wind shear near the surface is seen in the v component profiles of the

cold-case composites. A less accentuated wind shear is present in the zonal component of the wind for both warm and cold cases. However, the vertical wind shear is more accentuated for the zonal when compared to the meridional component of the wind. These patterns indicate that the coldside of the BMC region presents a larger static stability. As a consequence, there is less mixing, and a more stratified MABL develops. This layer presents a stronger vertical shear at lower atmospheric levels compared to the warm part of the BMC region. At this warm region, the wind shear is less accentuated producing a more turbulent and mixed MABL.

4.3. Near-Surface Fluxes

[34] The collected data by the ship-borne meteorological station of OSS *Ary Rongel* were used to estimate the surface turbulent flux calculations. Measured SST$_{bulk}$, Wind$_{ship}$, T$_{ship}$, SLP, and RH are also included in the analysis here. Negative values of the heat fluxes indicate fluxes from the sea surface toward the atmosphere. The atmospheric boundary layer stability parameter at 10 m height (ζ) was multiplied by 10^2.

[35] Figures 5 and 6 show the near-surface data and estimates for all the particular experiments (OP23 to OP26). The wind speed displays some common features of variability from year to year as seen in Figure 5. On the northernmost part of the domain, the wind speed presents values ranging from 5 m s^{-1} (OP24 and OP26) to 15 m s^{-1} (OP25). After this starting point, wind speeds begin to gradually increase when the air is lying over the BC (warmside) and near to the BMC oceanic front. The maximum wind speed values at the BC side range from 11 m s^{-1} (OP26) to 23 m s^{-1} (OP25). All measurements show that wind speed tends to decrease fairly slowly while crossing the BC/MC front (denoted by the vertical line in the graph) and when over the colder waters at the MC domain. In some cases an abrupt decline in wind speed is observed (as in OP23). The wind speed has dropped down from 10 m s^{-1} to 6 m s^{-1}. At the cold BMC side the maximum wind speeds vary from 5 m s^{-1} registered in OP23 to 11 m s^{-1} in OP25. It is interesting to note that in OP25 even over cold waters the wind speed has increased southward of the BC/MC front. This could be due to the large-scale circulation phenomena rather than the local SST modulation. However, even with this increase the wind speed is still small compared to that of the warm BC/MC side. It is more intense over the northern part of the domain, where the warm waters are located. Over the cold waters, the wind is less intense, so the reduction in wind stress is associated to the air-sea uncoupling under stable profiles as seen in section 5.2. This fact is also confirmed through the stability indexes analyses later in this section.

[36] The near-surface stability parameter SST$_{bulk}$ − T_{ship} clearly shows in Figure 5 that sea surface temperature affects the MABL near-surface stability. This parameter shows positive values over the warmside of the BC/MC front, meaning that the sea surface is acting as a heat source to the atmosphere. At the coldside, the opposite situation occurs. A colder ocean than the near-surface air allows a more stable MABL. In particular, the colder surface water will induce the formation of a stable mixed layer that decouples the upper MABL (as discussed in section 4.2)
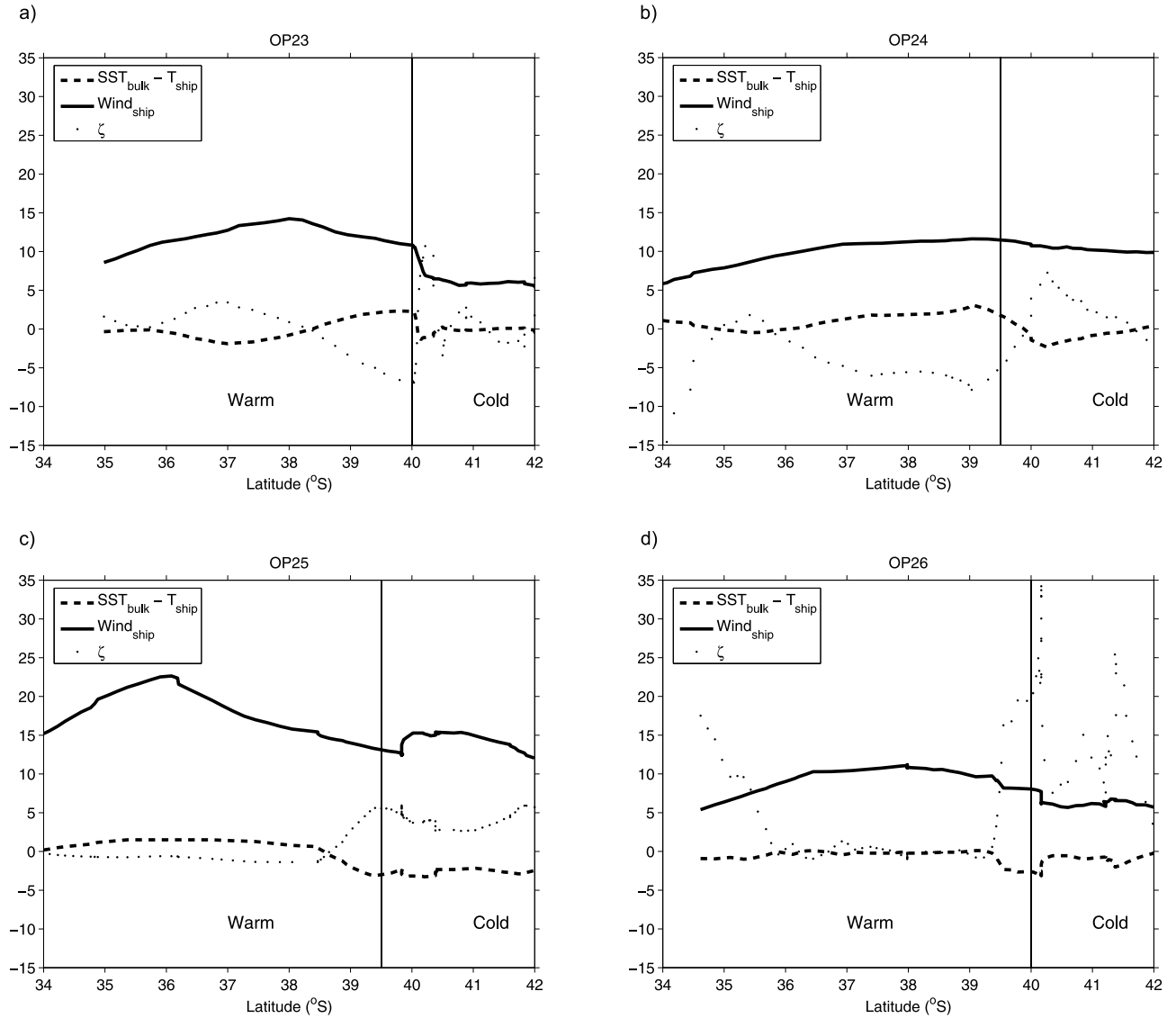
Figure 5. Synoptic, in situ measurements taken along OSS *Ary Rongel* routes for (a) OP23, (b) OP24, (c) OP25, and (d) OP26. (Wind$_{ship}$): wind speed measured at the vessel; (SST$_{bulk}$ − T$_{ship}$) stability parameters (°C); Q_T: total heat fluxes (×10 W m^{-2}); ζ: atmospheric stability parameter (×10^2). All information is derived from the ship-borne meteorological data. The vertical lines denote approximately the Brazil Current (BC)/Malvinas (Falkland) Current (MC) front position.

indicating a reduction of the vertical mixing. The near-surface stability conditions verified in this analysis are also verified by ζ calculations. The ζ results have negative (positive) values north (south) of the BC/MC confluence, which points to unstable (stable) conditions of the lower atmosphere. The spatial distribution of ζ is in reasonable agreement with the SST$_{bulk}$ − T$_{ship}$ calculations.

[37] The total heat fluxes vary approximately from −215 W m^{-2} to 50 W m^{-2}. These estimates, as well as their spatial variability, are in fair agreement with the climatology presented by *Tokinaga et al.* [2005]. For all experiments the maximum Q_T estimates are distributed between 35°S and 39°S, for all Q_S, Q_L, and Q_T, approximately. The larger fluxes values found at the warmside are associated with the larger air-sea temperature differences and wind speeds occurring at this region (see also Table 3).

This feature is characteristic of the region where the MABL is unstable and flux exchanges are intense. Conversely, at the coldside of the confluence, Q_T is reduced to values ranging from −20 W m^{-2} (OP24) to 60 W m^{-2} (OP25). This reduction is also associated with the lower SST and wind speed found in this region (Figures 5 and 7). During OP25 and OP26 the energy fluxes at the coldside of the oceanic front were directed downward. During these two experiments, northerly winds blew at the confluence, driving a warm-air advection toward the south and then creating a very stable boundary layer at the coldside.

[38] The mean fluxes estimated over the warmside of the BMC are generally higher than those obtained on the coldside. As it should be expected, the warmside releases more energy toward the atmosphere because of the higher SST and stronger wind speed, driving a more unstable
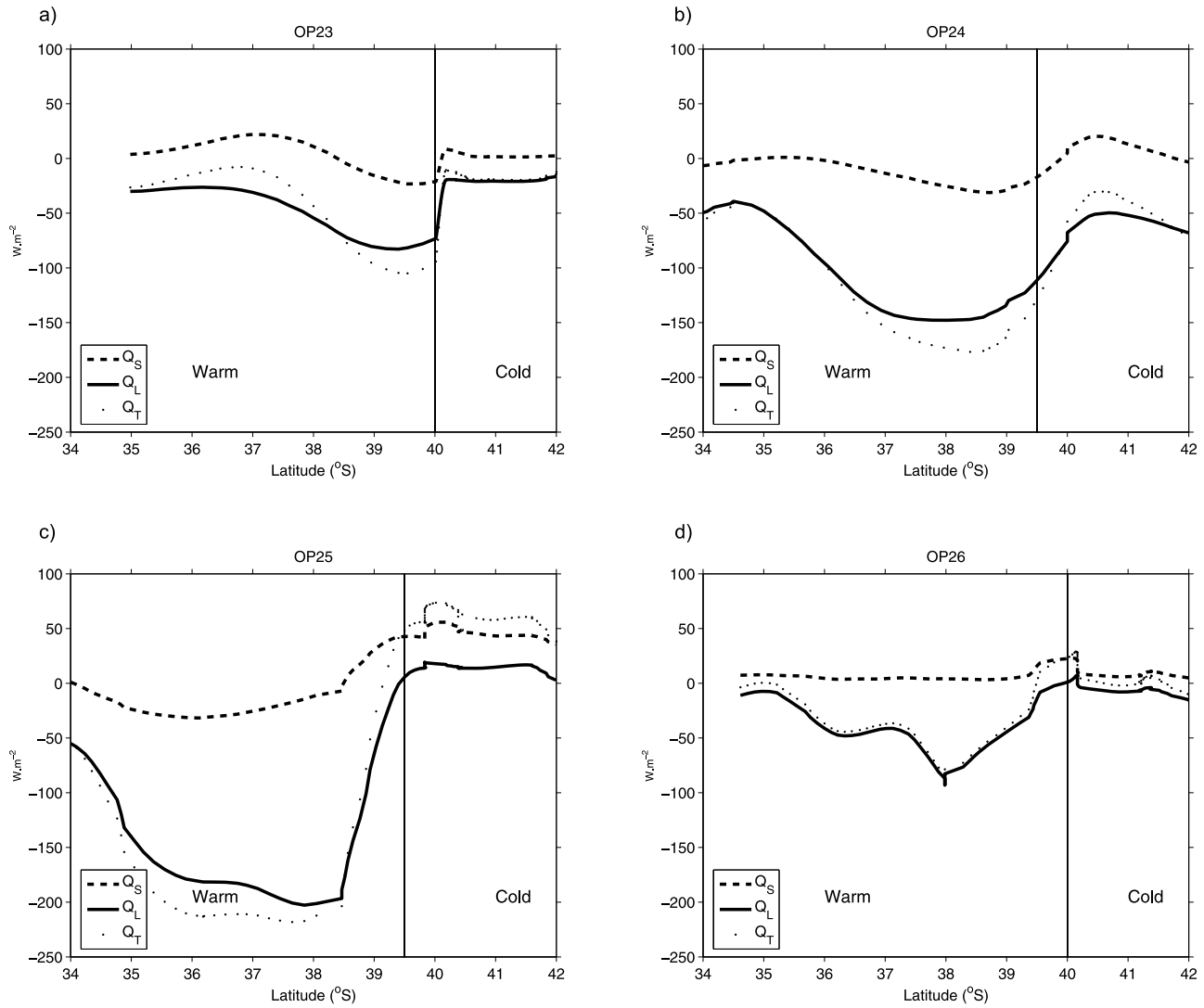
Figure 6. Synoptic in situ measurements taken along OSS *Ary Rongel* routes for (a) OP23, (b) OP24, (c) OP25, and (d) OP26. Q_S: sensible heat fluxes ($\times 10$ W m^{-2}); Q_L: latent heat fluxes ($\times 10$ W m^{-2}). All information is derived from the ship-borne meteorological data. The vertical lines denote approximately the BC/MC front position.

MABL. At the coldside of the front the behavior is opposite. The flux results presented here are consistent with previous studies at other oceanic fronts such as the Agulhas Current region [*Rouault et al.*, 2000] and the eastern equatorial Pacific [*Chelton et al.*, 2001; *Hashizume et al.*, 2002; *Pezzi et al.*, 2004; *Seo et al.*, 2007]. The agreement is also noticeable when we compare our synoptic flux estimates with the climatology of *Tokinaga et al.* [2005] for the BMC region. All the above-mentioned studies were performed aiming to understand the effects of SST on the vertical MABL mixing modulation. Integrated analyses of the lower boundary conditions such as SST, heat fluxes, and MABL vertical structure (wind shear) provide strong evidence that at the BMC region is a crucial mechanism in the ocean-atmosphere system. The evidence of reduction (increase) of the wind shear and strengthening (weakening) of the surface wind speed over the warm (cold) waters is consistent with the static stability mechanism proposed in previous studies [*Hayes et al.*, 1989; *Wallace et al.*, 1989].

4.4. In Situ SLP

[39] The role of SLP on modulating the surface wind speed is still an open question in the scientific community. This was recently emphasized by the comprehensive review made by *Small et al.* [2008]. *Lindzen and Nigam* [1987] suggested a hypothesis attributing the surface wind adjustments to variations of the SLP gradients caused by the difference in air temperature on either side of an oceanic front. According to their hypothesis, a lower SLP is expected over regions of warm waters while higher SLP are to be found over colder waters. As a consequence, stronger winds would be found where the lowest pressure or SST gradients are located. The cross-frontal, ship-borne measurements of SST$_{bulk}$ and SLP for OP23 to OP26 are presented in Figure 7. As expected, lower SLP values were indeed found on the warm part of the BC/MC front during OP23 and OP24. SLP over the warmside of the front ranges from 1016 hPa at 35°S decreasing to 1010 hPa at 39°S. After crossing the frontal region, SLP raises up again to
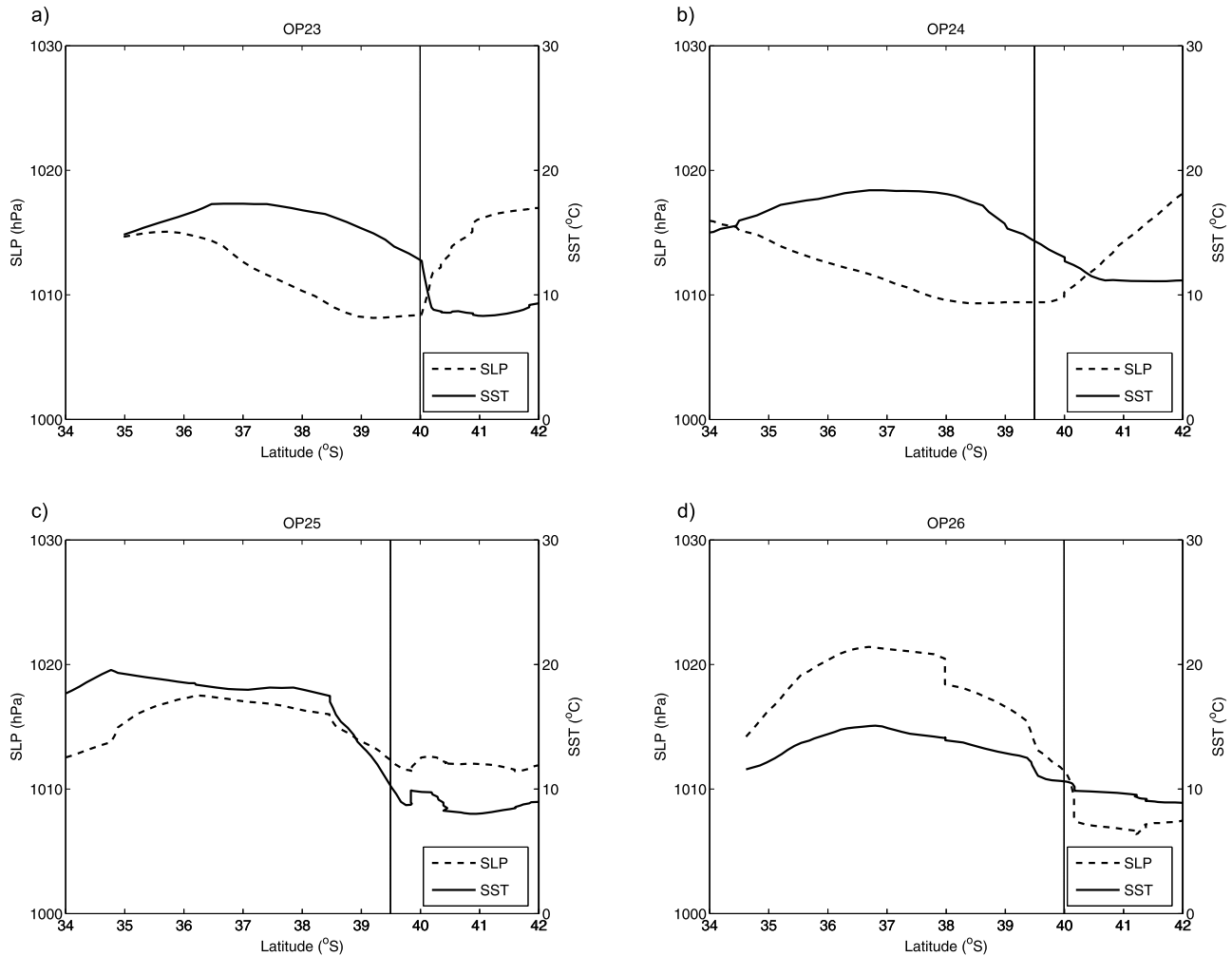
Figure 7. Synoptic, in situ measurements taken along OSS *Ary Rongel* routes for (a) OP23, (b) OP24, (c) OP25, and (d) OP26. SLP, sea-level pressure measured at the vessel; SST, sea surface temperature (°C). The vertical line approximately denotes the BC/MC front position.

1006 hPa near 41°S. During OP25 and OP26, however, the SLP presented an opposite behavior. High pressure occurs over the warmside of the front with values ranging from 1017 hPa (OP25) up to 1022 hPa (OP26). Over the cold-side, SLP drops down to 1011 hPa and 1005 hPa for OP25 and OP26, respectively. These data, measured by the barometer onboard the ship (Figure 7), are confirmed by the radiosonde data (Table 3).

[40] Most of the observed SLP changes across the confluence are, in fact, determined by the synoptic configuration of the atmosphere. Figure 2 shows a broader-scale pattern. Nevertheless, the questions about how much of the hydrostatic MABL adjustments are caused by the local SST modulation or by the synoptic scale systems still remain. In order to complement our analysis, we plotted smoothed latitude-height contours of the pressure perturbation individually for each expedition (Figure 8). At each level, the average pressure was removed, and then a "perturbation pressure" was computed with respect to the horizontal pressure average.

[41] In all cases except OP24 a reasonably large pressure gradient exists above the boundary layer, with higher pressure observed at lower latitudes (the warm sector).

Furthermore, all cases show an appreciable perturbation of the pressure gradient within the boundary layer. This perturbation is generally more intense at lower levels, indicating that it must be associated to surface-related processes. Besides these general agreements, some aspects are remarkably different among each of the experiments. During OP23, the confluence was responsible for weakening the pressure gradient within the boundary layer. In OP25 and OP26, on the other hand, the synoptic pressure gradient was intensified within the boundary layer. In OP24, despite the subtle synoptic pressure gradient, a well-defined pressure gradient induced by the oceanic front occurs within the boundary layer, with higher pressures at the coldside.

[42] *Tomas et al.* [1999] report that the MABL pressure perturbation beyond the synoptic forcing depends on two processes. First, the SST difference tends to generate lower pressures over the warmer side of the oceanic front and vice versa. However, the warmside boundary layer also tends to be thicker as noticed in our results (Figure 4a), being consequently denser than the free atmosphere air over a deeper column that occurs over the coldside. This process tends to induce higher pressures over the warm sector. Therefore, the final result will depend on which of the two
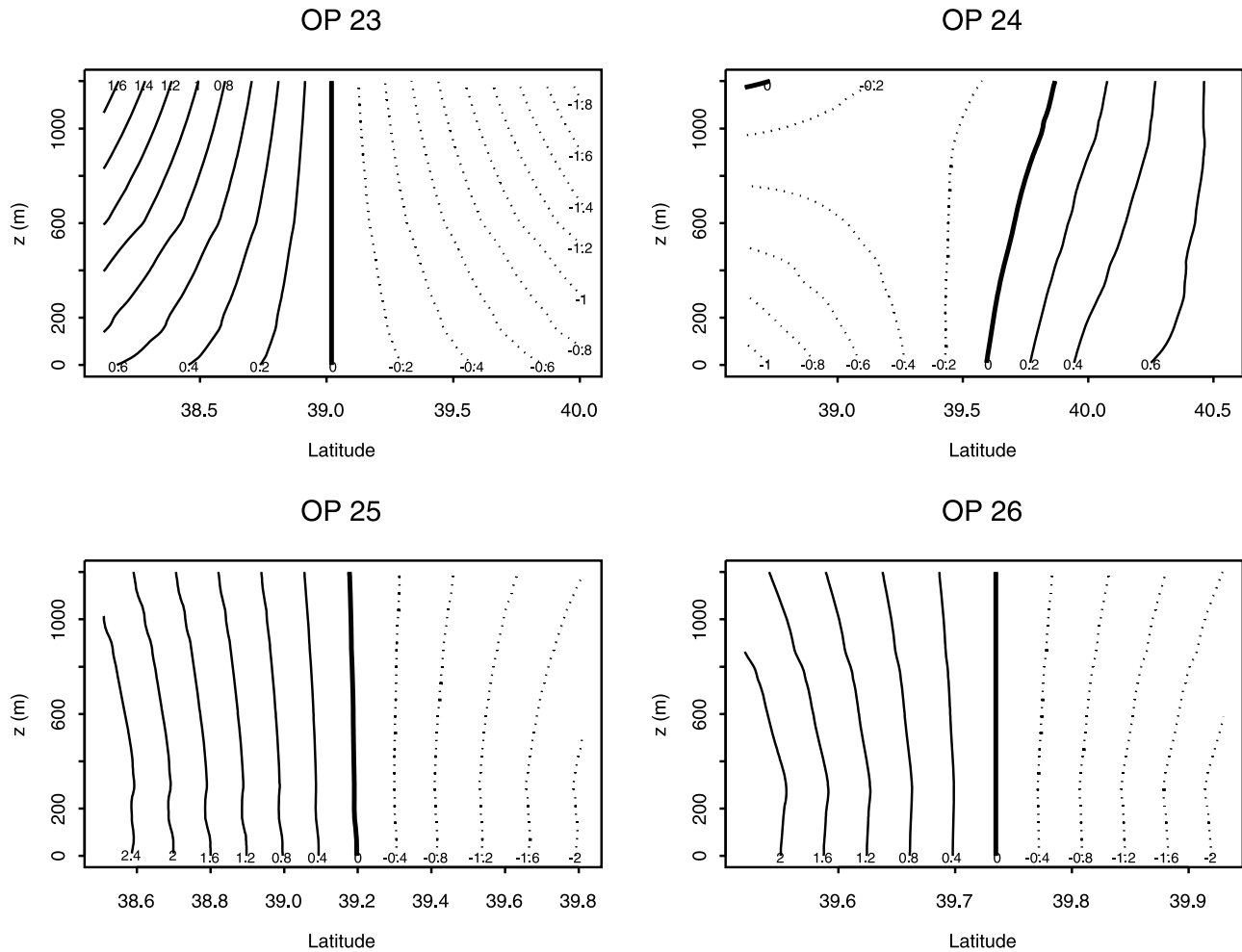
OP 23

OP 24

OP 25

OP 26

Figure 8. Smoothed latitude-height contours of pressure perturbation for the four experiments OP23, OP24, OP25, and OP26. The perturbations are determined with respect to the average pressure at each height. Contour units are in hPa.

processes is dominant. *Song et al.* [2006] and *Skyllingstad et al.* [2007] both suggested that in extratropical regions (such as the BMC), the boundary layer structure over an oceanic front will largely depends on the existing thermal advection pattern of the atmosphere.

[43] In the case of cold-air advection (cold air coming from the south of the BC/MC front) during our experiments, a mixed layer occurs at the coldside of the front. The advected cold air enhances the vertical air temperature gradients and, consequently, the sensible heat fluxes over the warmside of the front. This configuration results in a thicker, warmer boundary layer over the warm sector compared to that of the cold sector. Such a configuration, with cold-air advection across the confluence, for instance, happened during OP24. In this case, the coldside mixed layer was approximately 500 m thick, with a mean potential temperature of 281.75 K. Over the warmside of the oceanic front, the mixed layer was 700 m high, associated to a mean potential temperature of 283.25 K (Table 2). Such temperature difference over a moderately deep boundary layer is enough to dominate over the influence caused by the thickness effect. Therefore, the cold-air advection, prevalent in OP24, is responsible for positive (negative) pressure perturbations over the coldside (warmside) of the BMC. A

similar process occurred during OP23. In that case, the pressure perturbations locally induced at the BMC oppose the existing synoptic pressure gradient, reducing it at lower levels.

[44] In contrast, when warm-air advection (warm air coming from the north of the BC/MC front) exists across the BMC region, the mixed layer exists only over the warm sector. In the cold portion, a shallow, highly stable boundary layer is produced as a consequence of downward sensible heat fluxes. Despite being appreciably colder than the warm portion, such a stable boundary layer is shallower than the mixed layer occurring over the warmside. In that case, the thickness effect dominates over the atmospheric temperature effect, and the SST gradients are responsible for positive (negative) pressure perturbations over the warmside (coldside) of the BC/MC front. Cases of warm-air advection were observed during OP25 and OP26, when northward meridional winds prevailed. In both cases, the pressure perturbation enhanced the existent synoptic gradient, as shown in Figure 8.

[45] In a large-eddy simulations study, *Skyllingstad et al.* [2007] investigated the flow across an oceanic front for both cases of cold and warm thermal advection. Their results confirm the description above made for our observations. In

a warm-air advection case, a negative pressure perturbation occurs over the cold portion of an oceanic front. In opposition to that, a cold-air advection determines a positive pressure perturbation over the cold portion. *Skyllingstad et al.* [2007], however, do not explain their pattern differences, but *Tomas et al.* [1999] clarifies the issue. In conclusion, our observations, together with the theory proposed by *Tomas et al.* [1999] and the numerical simulations by *Skyllingstad et al.* [2007] comprise a good set of evidence to demonstrate how thermal advection drives a pressure gradient across oceanic fronts. For emphasizing that conclusion, a very simple conceptual model can be inferred, directly associating the type of advection to the sign of the pressure perturbation across the BC/MC front.

5. Concluding Remarks

[46] This work analyzed and discussed simultaneous oceanic and atmospheric data collected during four experiments carried out by the INTERCONF program at the BMC region. This work extends and complements the study of *Pezzi et al.* [2005] where only data from November 2005 were available. To our knowledge, this is the only systematic observational ocean-atmosphere sampling effort conducted at the Brazil-Malvinas Confluence region so far. Despite the fact that this region is acknowledged as one of the most energetic regions of the world ocean, very few studies have addressed the importance of studying the air-sea coupling processes there. Our results indicate the presence of lateral SST gradients at BMC as high as $0.3°C \, km^{-1}$ at surface and subsurface. Vertical water temperature gradients are on the order of $0.08°C \, m^{-1}$ at depths of $400-500$ m.

[47] Analyzing the MABL-OBL coupling during four cruises between 2004 and 2007, this work offered elements to conclude that the MABL is modulated by the strong temperature gradients present at the sea surface of the study area. An explanation for this modulation lies in the fact that the MABL in the BMC region adjusts itself to the SST modifications characteristic from oceanic frontal regions, as already reported for other areas of the world ocean such as the equatorial Pacific and the Agulhas Current region. Over warm waters, the static instability and the turbulence within the MABL are both increased. Still over warm waters, our data indicated a reduction in the wind shear as well as an enhancement of the surface winds at the MABL. Over the coldside of the BMC region, the MABL is more stable and is associated to an increased wind shear, resulting in weaker surface winds. Both situations are in close agreement with results presented by *Wallace et al.* [1989] for the eastern equatorial Pacific Ocean. This process was already proposed as an explanation for the air-sea coupling at other frontal regions of the world ocean as described in the very recent review paper by *Small et al.* [2008]. For our study region, the mean MABL structure was thicker over the warmside (BC) than over the coldside (MC) of the confluence. The warmside displayed systematically larger h_0 values compared to the coldside. The surface Q_S and Q_L fluxes always increased from the cold to the warmside of the oceanic front owing to the increase of the wind and temperature (q) difference between the sea surface and the air.

[48] Some interesting points arose from the results of our observational effort. Our analysis suggests that the SLP was locally modulated the surface condition during all experiments. The static stability vertical mixing mechanism explains this modulation. This was clearly observed in OP23 and OP24, where lower (higher) SLP values are located over warm (cold) waters (Figures 7a and 7b). Nevertheless, the BMC SST gradients also modulated the synoptic pressure gradient observed during OP25 and OP26. However, in these last cases, the SLP leaded an opposite role, driving lower pressures at the coldside and higher pressures at the warmside. Different results are reported by *de Szoeke and Bretherton* [2004] and *Small et al.* [2005]. For addressing this issue, we should bear in mind that the southwestern Atlantic Ocean is a cyclone and anticyclone track region [*Hoskins and Hodges*, 2005]. This fact distinguishes this region from most of better previously studied frontal oceanic regions, which are located in the tropics. We suggest that the presence of large scale synoptic system affects the SLP modulation at the Brazil-Malvinas Confluence region. The effects of postfrontal and prefrontal conditions can result in opposite advective patterns of the atmosphere in the region.

[49] To better investigate all these complex interactions between the local and the large-scale processes, oceanic and atmospheric models should be employed. Numerical modeling can complement our observational results in the future, as well as being useful for directing new experiments toward particular regions of our study area. Both *de Szoeke and Bretherton* [2004] and *Small et al.* [2005] offered a similar approach for studying the equatorial Pacific Ocean. Long numerical integrations (e.g., seasonal simulations covering a large scale) may permit us to isolate the effects of the large-scale signals from the local SST one, and then we can check whether the hydrostatic stability is a relevant player in the MABL stability process when a synoptic system is active over the BMC region or, on the other hand, it is negligible compared to the large-scale (pressure) signal.

[50] We finish by remarking that the southwestern Atlantic Ocean is a very important region for the weather and climate of South America, since it is a path for atmospheric frontal and storm tracks and cyclone generation and intensification. We expect that new, consistent efforts to better study and understand the air-sea coupling in the BMC region can benefit from the results presented here. It is expected that, in the future, a continuous observing program for studying the air-sea coupling processes in the southwestern Atlantic region can be established.

References

Albrecht, B. A., M. P. Jensen, and W. J. Syrett (1995), Marine boundary layer structure and fractional cloudiness, *J. Geophys. Res.*, *100*, 14,209–14,222.

Bianchi, A. A., A. R. Piola, and G. J. Collino (2002), Evidence of double diffusion in the Brazil-Malvinas Confluence, *Deep Sea Res., Part I*, *49*, 41–52, doi:10.1016/S0967-0637(01)00039-5.

Caltabiano, A. C., I. S. Robinson, and L. Pezzi (2005), Multi-year satellite observations of instability waves in the tropical Atlantic Ocean, *Ocean Sci. Disc.*, *2*, 1–35.

Castro, B. M., J. A. Lorenzzetti, I. C. A. Silveira, and L. B. Miranda (2006), Estrutura termohalina e circulação na região entre o Cabo de São Tomé (RJ) e o Chuí (RS), in *O ambiente oceanográfico da plataforma continental e do talude na região Sudeste-Sul do Brasil*, edited by C. L. del Bianco Rossi-Wongtschowski and L. Saint-Pastous Madureira, pp. 11–120, EDUSP, São Paulo, Brazil.

Chelton, D. B., and F. J. Wentz (2005), Global microwave satellite observations of sea-surface temperature for numerical weather prediction and climate research, *Bull. Am. Meteorol. Soc.*, *86*, 1097–1115, doi:10.1175/BAMS-86-8-1097.

Chelton, D. B., M. G. Schlax, D. L. Witter, and J. G. Richman (1990), GEOSAT altimeter observations of the surface circulation of the Southern Ocean, *J. Geophys. Res.*, *95*, 17,877–17,903, doi:10.1029/JC095iC10p17877.

Chelton, D. B., F. J. Wentz, C. L. Gentemann, R. A. de Szoeke, and M. G. Schlax (2000), Satellite microwave SST observations of transequatorial tropical instability waves, *Geophys. Res. Lett.*, *27*(9), 1239–1242, doi:10.1029/1999GL011047.

Chelton, D. B., S. K. Esbensen, M. G. Schlax, N. Thun, M. Freilich, F. J. Wentz, C. L. Gentemann, M. J. McPhaden, and P. S. Schopf (2001), Observations of coupling between surface wind stress and sea surface temperature in the eastern tropical Pacific, *J. Clim.*, *14*, 1479–1498, doi:10.1175/1520-0442(2001)014<1479:OOCBSW>2.0.CO;2.

de Szoeke, S. P., and C. S. Bretherton (2004), Quasi-Lagrangian large eddy simulation of cross-equatorial flow in the East Pacific atmospheric boundary layer, *J. Atmos. Sci.*, *61*, 1837–1858, doi:10.1175/1520-0469(2004)061<1837:QLESOC>2.0.CO;2.

Fairall, C. W., E. F. Bradley, D. P. Rogers, J. B. Edson, and G. S. Young (1996), Bulk parameterization of air-sea fluxes for Tropical Ocean-Global Atmosphere Coupled-Ocean Atmosphere Response Experiment, *J. Geophys. Res.*, *101*, 3747–3764, doi:10.1029/95JC03205.

Fairall, C. W., E. F. Bradley, J. E. Hare, A. A. Grachev, and J. B. Edson (2003), Bulk parameterization of air-sea fluxes: Updates and verification for the COARE algorithm, *J. Clim.*, *16*, 571–591, doi:10.1175/1520-0442(2003)016<0571:BPOASF>2.0.CO;2.

Fisch, G., J. Tóta, L. A. T. Machado, M. A. F. Silva Dias, R. F. da F. Lyra, C. A. Nobre, A. J. Dolman, and J. H. C. Gash (2004), The convective boundary layer over pasture and forest in Amazonia, *Theor. Appl. Climatol.*, *78*(1–3), 47–59, doi:10.1007/s00704-004-0043-x.

Gan, M. A., and V. B. Rao (1991), Surface cyclogenesis over South America, *Mon. Weather Rev.*, *119*, 1293–1302, doi:10.1175/1520-0493(1991)119<1293:SCOSA>2.0.CO;2.

Garcia, C. A. E., Y. V. B. Sarma, M. M. Mata, and V. M. T. Garcia (2004), Chlorophyll variability and eddies in the Brazil-Malvinas Confluence region, *Deep Sea Res.*, *51*, 159–172, doi:10.1016/j.dsr2.2003.07.016.

Garzoli, S. L., and Z. Garraffo (1989), Transports, frontal motions and eddies at the Brazil-Malvinas Currents confluence, *Deep Sea Res., Part A*, *36*, 681–703, doi:10.1016/0198-0149(89)90145-3.

Hashizume, H., S. P. Xie, W. T. Liu, and K. Takeuchi (2001), Local and remote atmospheric response to tropical instability waves: A global view from space, *J. Geophys. Res.*, *106*, 10,173–10,185, doi:10.1029/2000JD900684.

Hashizume, H., S.-P. Xie, M. Fujiwara, M. Shiotani, T. Watanabe, Y. Tanimoto, W. T. Liu, and K. Takeuchi (2002), Direct observations of atmospheric boundary layer response to SST variations associated with tropical instability waves over the eastern equatorial Pacific, *J. Clim.*, *15*, 3379–3393, doi:10.1175/1520-0442(2002)015<3379:DOOABL>2.0.CO;2.

Hayes, S. P., M. J. McPhaden, and J. M. Wallace (1989), The influence of sea surface temperature on surface wind in the eastern equatorial Pacific: Weekly to monthly variability, *J. Clim.*, *2*, 1500–1506, doi:10.1175/1520-0442(1989)002<1500:TIOSST>2.0.CO;2.

Hoskins, B. J., and K. I. Hodges (2005), A new perspective on Southern Hemisphere storm tracks, *J. Clim.*, *18*, 4108–4129, doi:10.1175/JCLI3570.1.

Legeckis, R., and A. L. Gordon (1982), Satellite observations of the Brazil and Falkland Currents: 1975 to 1976 and 1978, *Deep Sea Res.*, *29*, 375–401, doi:10.1016/0198-0149(82)90101-7.

Lindzen, R. S., and S. Nigam (1987), On the role of sea surface temperature gradients in forcing low-level winds and convergence in the tropics, *J. Atmos. Sci.*, *44*(17), 2418–2436, doi:10.1175/1520-0469(1987)044<2418:OTROSS>2.0.CO;2.

Liu, W., X. Xie, P. S. Polito, S. P. Xie, and H. Hashizume (2000), Atmospheric manifestation of tropical instability wave observed by QuickSCAT and tropical rain measuring mission, *Geophys. Res. Lett.*, *27*(16), 2545–2548, doi:10.1029/2000GL011545.

O'Neill, L. W., D. B. Chelton, and S. K. Esbensen (2003), Observations of SST-induced perturbations of the wind stress field over the Southern Ocean on seasonal time scales, *J. Clim.*, *16*, 2340–2354, doi:10.1175/2780.1.

Panofsky, H., and J. A. Dutton (1984), *Atmospheric Turbulence*, 397 pp., Wiley-Intersci., New York.

Pezzi, L. P., and K. J. Richards (2003), Effects of lateral mixing on the mean state and eddy activity of an equatorial ocean, *J. Geophys. Res.*, *108*(C12), 3371, doi:10.1029/2003JC001834.

Pezzi, L. P., J. Vialard, K. J. Richards, C. Menkes, and D. Anderson (2004), Influence of ocean atmosphere coupling on the properties of tropical instability waves, *Geophys. Res. Lett.*, *31*, L16306, doi:10.1029/2004GL019995.

Pezzi, L. P., R. B. Souza, M. S. Dourado, C. A. E. Garcia, M. M. Mata, and M. A. F. Silva-Dias (2005), Ocean-atmosphere in situ observations at the Brazil-Malvinas Confluence region, *Geophys. Res. Lett.*, *32*, L22603, doi:10.1029/2005GL023866.

Piola, A. R., and R. P. Matano (2001), Brazil and Falklands (Malvinas) currents, in *Encyclopedia of Ocean Sciences*, edited by S. A. Thorpe, pp. 340–349, Elsevier, New York.

Polito, P., J. P. Ryan, W. T. Liu, and F. P. Chavez (2001), Oceanic atmospheric anomalies of tropical instability waves, *Geophys. Res. Lett.*, *28*(11), 2233–2236, doi:10.1029/2000GL012400.

Pyatt, H. E., B. A. Albrecht, C. Fairall, J. E. Hare, N. Bond, P. Minnis, and J. K. Ayers (2005), Evolution of marine atmospheric boundary layer structure across the Cold Tongue–ITCZ Complex, *J. Clim.*, *18*, 737–753, doi:10.1175/JCLI-3287.1.

Richards, K. J., and N. Edwards (2003), Lateral mixing in the equatorial Pacific: The importance of inertial instability, *Geophys. Res. Lett.*, *30*(17), 1888, doi:10.1029/2003GL017768.

Rouault, M., A. M. Lee-Thorp, and Lutjeharms (2000), The atmospheric boundary layer above the Agulhas Current during alongcurrent winds, *J. Phys. Oceanogr.*, *30*, 40–50, doi:10.1175/1520-0485(2000)030<0040:TABLAT>2.0.CO;2.

Santos, L. A. R. (2005), Análise e carcterização da camada limite convectiva em área de pastagem, durante o período de transição entre a estação sea e chuvosa na Amazônia (Experimento RaCCI-LBA), 118 pp., INPE-551.5510.522. M. Sci. Diss. in Meteorol., INPE, São José dos Campos, Brazil.

Saraceno, M., C. Provost, A. R. Piola, J. Bava, and A. Gagliardini (2004), Brazil Malvinas Frontal System as seen from 9 years of advanced very high resolution radiometer data, *J. Geophys. Res.*, *109*, C05027, doi:10.1029/2003JC002127.

Seo, H., M. Jochum, R. Murtugudde, A. J. Miller, and J. O. Roads (2007), Feedback of tropical instability-wave-induced atmospheric variability onto the ocean, *J. Clim.*, *20*, 5842–5855, doi:10.1175/JCLI4330.1.

Skyllingstad, E. D., D. Vickers, L. Mahrt, and R. Samelson (2007), Effects of mesoscale sea surface temperature fronts on the marine atmospheric boundary layer, *Boundary Layer Meteorol.*, *123*, 219–237, doi:10.1007/s10546-006-9127-8.

Small, R. J., S.-P. Xie, Y. Wang, S. K. Esbensen, and D. Vickers (2005), Numerical simulation of boundary layer structure and cross-equatorial flow in the eastern Pacific, *J. Atmos. Sci.*, *62*, 1812–1830, doi:10.1175/JAS3433.1.

Small, R. J., S. P. de Szoeke, S. P. Xie, L. O'Neill, H. Seo, Q. Song, P. Cornillon, M. Spall, and S. Minobe (2008), Air-sea interaction over ocean fronts and eddies, *Dyn. Atmos. Oceans*, *45*, 274–319, doi:10.1016/j.dynatmoce.2008.01.001.

Smith, S. D., C. W. Fairall, G. L. Geernaert, and L. Hasse (1996), Air-sea fluxes: 25 years of progress, *Boundary Layer Meteorol.*, *78*, 247–290, doi:10.1007/BF00120938.

Song, Q., P. Cornillon, and T. Hara (2006), Surface wind response to oceanic fronts, *J. Geophys. Res.*, *111*, C12006, doi:10.1029/2006JC003680.

Souza, R. B., M. M. Mata, C. A. E. Garcia, M. Kampel, E. N. Oliveira, and J. A. Lorenzzetti (2006), Multi-sensor satellite and in situ measurements of a warm core eddy south of the Brazil-Malvinas Confluence region, *Remote Sens. Environ.*, *100*, 52–66, doi:10.1016/j.rse.2005.09.018.

Spall, M. A. (2007), Effect of sea surface temperature-wind stress coupling on baroclinic instability in the ocean, *J. Phys. Oceanogr.*, *37*, 1092–1097, doi:10.1175/JPO3045.1.

Stull, R. B. (1988), *An Introduction to Boundary Layer Meteorology*, 666 pp., Kluwer Acad. Publ., Dordrecht, Netherlands.

Tomas, R. A., J. R. Holton, and P. J. Webster (1999), The influence of cross-equatorial pressure gradients on the location of near-equatorial convection, *Q. J. R. Meteorol. Soc.*, *125*, 1107–1127, doi:10.1256/smsqj.55602.

Tokinaga, H., Y. Tanimoto, and S.-P. Xie (2005), SST-induced wind variations over Brazil-Malvinas confluence: Satellite and in-situ observations, *J. Clim.*, *18*, 3470–3482, doi:10.1175/JCLI3485.1.

Wallace, J. M., T. P. Mitchell, and C. J. Deser (1989), The influence of sea-surface temperature on surface wind in the eastern equatorial Pacific: Weekly to monthly variability, *J. Clim.*, *2*, 1492–1499, doi:10.1175/1520-0442(1989)002<1492:TIOSST>2.0.CO;2.

Wentz, F. J., C. Gentemann, and P. Ashcroft (2003), On-orbit calibration of AMSR-E and the retrieval of ocean products, 83rd AMS Annual Meeting, Am. Meteorol. Soc., Long Beach, Calif., 9–13 February.

Xie, S. P. (2004), Satellite observations of cool ocean-atmosphere interaction, *Bull. Am. Meteorol. Soc.*, *85*, 195–208, doi:10.1175(BAMS-82–2-195).

––––––––––––––––––

O. Acevedo, Department of Physics, UFSM, Campus da UFSM, Avenida Roraima 1000, Camobi Caixa Postal 5021, Santa Maria, CEP 97105-970, Brazil.

R. de Camargo, IAG, USP, Rua do Matão 1226, São Paulo, CEP 05508-090, Brazil.

R. B. de Souza, CRS, INPE, Campus da UFSM, Avenida Roraima 1000, Camobi Caixa Postal 5021, Santa Maria, CEP 97105-970, Brazil.

C. A. E. Garcia and M. M. Mata, Ocean and Climate Studies Laboratory, Institute of Oceanography, FURG, Avenida Itália Km 08, Rio Grande, 96201-900, Brazil.

L. P. Pezzi, OBT, INPE, Avenida dos Astronautas 1758, Jardim da Granja, São José dos Campos, 12227-010, Brazil. (luciano@dsr.inpe.br)

I. Wainer, Department of Physical Oceanography, USP, Praça do Oceanográfico 191, São Paulo, 05508-120, Brazil.